A kinetic account for amphetamine-induced monoamine release

Peter S. Hasenhuetl,* Shreyas Bhat,* Felix P. Mayer, Harald H. Sitte, Michael Freissmuth, and Walter Sandtner

Institute of Pharmacology and the Gaston H. Glock Research Laboratories for Exploratory Drug Development, Center of Physiology and Pharmacology, Medical University of Vienna, Vienna, Austria

The plasmalemmal monoamine transporters for dopamine, norepinephrine, and serotonin (SERT) are targets for amphetamines. In vivo, amphetamines elicit most, if not all, of their actions by triggering monoamine efflux. This is thought to be accomplished by an amphetamine-induced switch from the forward-transport to the substrate-exchange mode. The mechanism underlying this switch has remained elusive; available kinetic models posit that substrates and cosubstrate Na^+ ions bind either in a random or in a sequential order. Neither can account for all reported experimental observations. We used electrophysiological recordings to interrogate crucial conformational transitions associated with the binding of five different substrates (serotonin, para-chloroamphetamine, and the high-affinity naphthyl-propan-amines PAL-287, PAL-1045, and PAL-1046) to human SERT expressed in HEK293 cells; specifically, we determined the relaxation kinetics of SERT from a substrate-loaded to a substrate-free state at various intracellular and extracellular Na^+ concentrations. These rates and their dependence on intracellular and extracellular Na^+ concentrations differed considerably between substrates. We also examined the effect of K^+ on substrate affinity and found that K^+ enhanced substrate dissociation. A kinetic model was developed, which allowed for random, but cooperative, binding of substrate and Na^+ (or K^+). The synthetic data generated by this model recapitulated the experimental observations. More importantly, the cooperative binding model accounted for the releasing action of amphetamines without any digression from alternating access. To the best of our knowledge, this model is the first to provide a mechanistic framework for amphetamine-induced monoamine release and to account for the findings that some substrates are less efficacious than others in promoting the substrate-exchange mode.

INTRODUCTION

The transport proteins for norepinephrine (SLC6A2), dopamine (SLC6A3), and serotonin (5-hydroxy-tryptamine [5-HT] and SLC6A4) terminate synaptic monoamine transmission by uptake of their cognate substrates into the presynaptic specialization (Kristensen et al., 2011). These proteins are secondary active transporters; substrate uptake is coupled to the electrochemical gradient of Na^+. Under physiological conditions, this vectorial, concentrative substrate uptake prevails; the transporter, which operates by an alternating access mechanism, binds the substrate and the cosubstrate ions in the outward-facing conformation, forms an occluded state, and opens an inner gate to produce the inward-facing state, which releases substrates and cosubstrates into the cytosol. The transporter completes the catalytic cycle by isomerization from the inward-facing to the outward-facing conformation in an empty state or by antiport of K^+ or H^+ (Nelson and Rudnick, 1979; Keyes and Rudnick, 1982). This has been referred to as forward-transport mode. In serotonin transporters (SERTs), intracellular K^+ and Na^+ have been shown to play opposing roles (Hasenhuetl et al., 2016); intracellular K^+ pushes the catalytic cycle into the forward-trans-

port mode. In contrast, intracellular Na^+ biases the system toward a second, distinct, transport mode. In this substrate-exchange mode, SERT oscillates between the substrate-loaded outward-facing and inward-facing conformations, but does not visit the conformations required to complete the catalytic cycle (Sitte and Freissmuth, 2015). The actions of amphetamines are thought to rely on this second transport mode; amphetamines are substrates and are hence transported into the cytosol, where they are exchanged for the physiological monoamine, which is translocated to the extracellular side. Thus, under the influence of amphetamines, the monoamine transporters shuttle through half cycles and support monoamine efflux, which accounts for most, if not all, of their biological actions (Sitte and Freissmuth, 2015).

Elevation of intracellular Na^+ plays an important role in promoting the substrate-exchange mode by imposing a brake on the forward-transport cycle (Hasenhuetl et al., 2016). In both dopamine transporters (DATs; Erreger et al., 2008) and SERT (Hasenhuetl et al., 2016), this has been adequately accounted for by sequential binding of substrate and Na^+. In a sequential order based on the first on/first off principle, Na^+ must bind

---

*P.S. Hasenhuetl and S. Bhat contributed equally to this paper.

Correspondence to Walter Sandtner: walter.sandtner@meduniwien.ac.at

P.S. Hasenhuetl's present address is Centre for Neural Circuits and Behaviour, University of Oxford, Oxford, England, UK.

first to the outward open state of the transporter before substrate binding and also be released before the translocated monoamine/amphetamine from the inward open state of the transporter. This is also consistent with molecular dynamics simulations, which indicate that Na^+ release from the inward-facing conformation is the first dissociation event (Razavi et al., 2017). However, sequential binding is incompatible with the action of amphetamines; elevation of intracellular Na^+ by ouabain (Bönisch, 1986), by the Na^+/H^+ ionophore monensin (Scholze et al., 2000), or via the patch pipette (Khoshbouei et al., 2003; Kahlig et al., 2005) enhances amphetamine-induced monoamine release. This can only be explained by a random order of substrate and Na^+ binding. This is because, in a sequential binding order, raising the intracellular Na^+ concentration ought to impede the dissociation of translocated amphetamine and thus blunt its monoamine-releasing action. This raises the question of whether amphetamines induce monoamine release by relying on the same conformational transitions observed under physiological conditions or by mechanisms distinct from alternating access (such as a substrate-conducting pore; Kahlig et al., 2005). We reasoned that the action of amphetamines could be explained without assuming any additional transport modes if the binding of substrate and Na^+ was random but cooperative; that is, Na^+ binding increases the affinity of the substrate and vice versa. This cooperative-binding model allows for the exchange of amphetamine and 5-HT on the inward-facing state of SERT even at high internal Na^+ concentrations while accounting for all the other observed physiological functions of SERT. We explored this model by relying on time-resolved measurements by patch-clamp recordings of specific conformational transitions induced by 5-HT and different amphetamines. We determined the effects of Na^+ and K^+ on the dissociation rates of different SERT substrates: 5-HT, *para*-chloroamphetamine (*p*-chloroamphetamine), the high-affinity partial releaser PAL-1045, and its congeners, PAL-287 and PAL-1046. Our observations are compatible with the assumption of cooperative binding in which Na^+ and substrate mutually enhance their affinity for the transporter to form a ternary complex. In addition, our data suggest that the binding of K^+ promotes substrate dissociation. A cooperative binding model was derived that recapitulated the present data in addition to a wide array of previously published results on physiological SERT function. We then tested whether this model was sufficient to explain amphetamine-induced substrate release. The model accounted qualitatively and quantitatively for the releasing action of amphetamines. Importantly, the model also provided an explanation for the phenomenon of partial release (i.e., the observation that some amphetamines are less efficacious than others in inducing monoamine efflux).

MATERIALS AND METHODS

Whole-cell patch clamp

Patch-clamp recordings were performed with human embryonic kidney (HEK293) cells expressing human SERT carrying an N-terminal green fluorescent protein tag under the control of a tetracycline-inducible expression system. Cells were seeded at low density for 24 h before the experiments. Substrate-induced human SERT currents were recorded under voltage-clamp conditions using the whole-cell patch-clamp technique.

Unless otherwise stated, the cells were continuously superfused with external solution containing 140 mM NaCl, 2.5 mM $CaCl_2$, 2 mM $MgCl_2$, 20 mM glucose, and 10 mM HEPES adjusted to pH 7.4 with NaOH (subsequently referred to as solution 1). In the experiments shown in Fig. 1, external Na^+ concentrations were varied by mixing a Na^+-free external solution (made by replacing 140 mM NaCl in external solution 1 with 140 mM NMDG chloride; pH was adjusted to 7.4 with NMDG) with the appropriate amount of solution 1. Variable external K^+ concentrations shown in Fig. 4 were made by adjusting NaCl, KCl, and NMDG chloride appropriately to match the concentrations displayed in the figure; constant osmolarity was maintained by using NMDG chloride.

Pipette solutions were prepared as described previously (Hasenhuetl et al., 2016; Bhat et al., 2017). The Na^+- and K^+-free pipette solution contained 143.5 mM Cl^-, 10 mM HEPES, 1 mM $CaCl_2$, 0.7 mM $MgCl_2$, 10 mM EGTA, and 140 mM NMDG chloride titrated to a pH of 7.2 using NMDG. A (high) Cl^- concentration of 143.5 mM was chosen for the experiments shown in Figs. 1 and 2 for two reasons. First, high internal Cl^- concentrations provided more stable recording conditions than low Cl^- concentrations when K^+ was omitted. Second, and more importantly, Cl^- and Na^+ have synergistic effects on ligand affinity, the extent of which varies with ligand identity (Humphreys et al., 1994). Thus, studying the effect of Na^+ on substrate binding requires saturating Cl^- concentrations. The concentration of Na^+ was varied, and osmolarity was kept constant by adjusting the concentration of NMDG chloride using NaCl (e.g., 10 mM NaCl + 130 mM NMDG chloride). For experiments using a high K^+ concentration (Fig. 3), 140 mM potassium methanesulfonate and 6 mM NaCl were used (including 10 mM HEPES, 1 mM $CaCl_2$, 0.7 mM $MgCl_2$, and 10 mM EGTA). Variable internal K^+ concentrations were obtained by mixing the pipette solution containing 140 mM K^+ with a solution containing NMDG methanesulfonate and 6 mM NaCl (including 10 mM HEPES, 1 mM $CaCl_2$, 0.7 mM $MgCl_2$, and 10 mM EGTA).

Currents were recorded at room temperature (20–24°C) using an Axopatch 200B amplifier and pClamp 10.2 software (MDS Analytical Technologies). Current
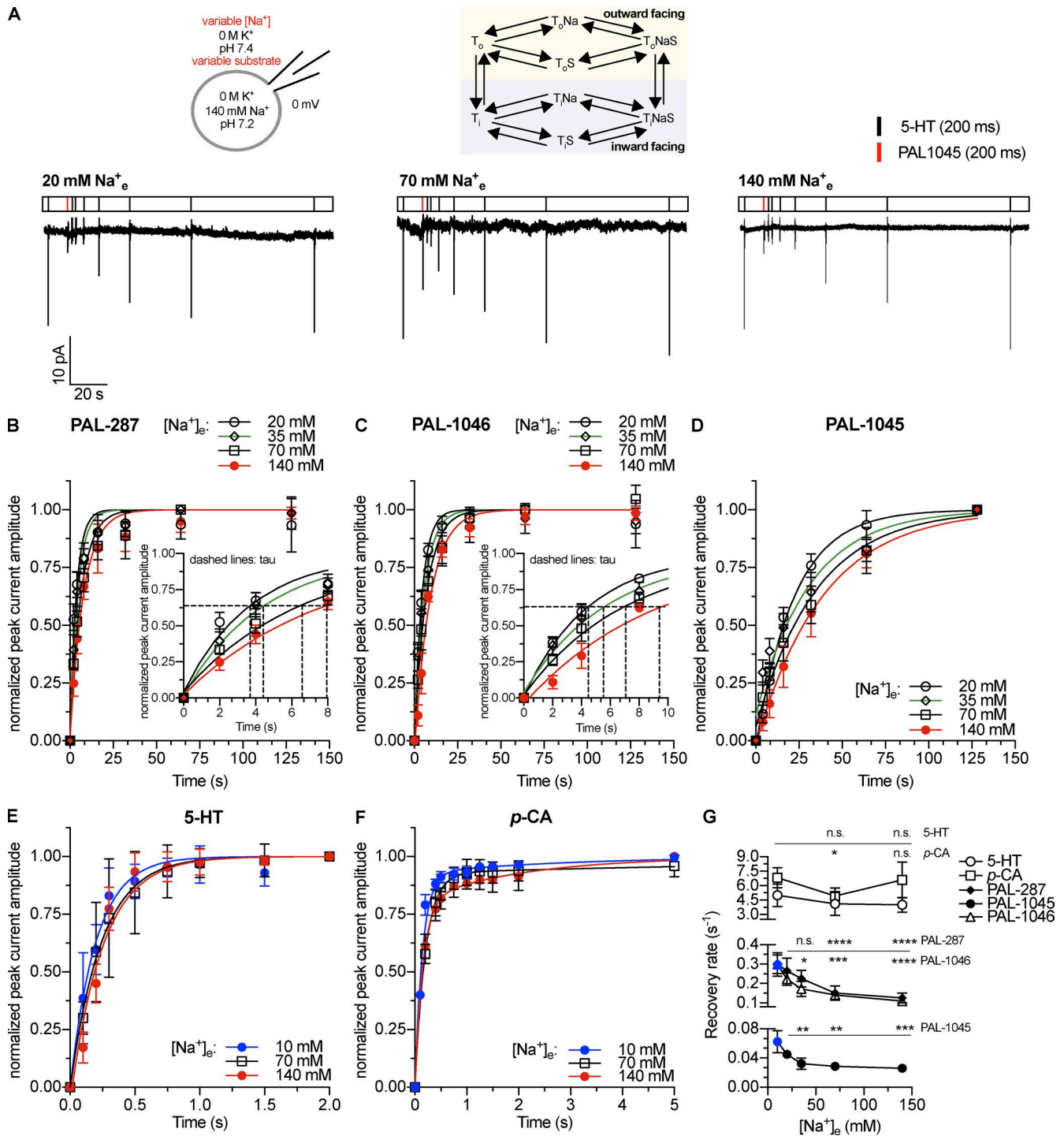
Figure 1. **Peak current recovery as a function of extracellular Na$^+$ concentration. (A)** Top: Schematic rendering of the recording conditions indicating the concentrations of intracellular and extracellular substrate and cosubstrate ions and reaction scheme of a Na$^+$-coupled transporter. Bottom: Original traces of representative experiments using 20, 70, or 140 mM extracellular Na$^+$. **(B–F)** Time-dependent recovery of 5-HT–induced (10 µM) peak current amplitude after application of 30 µM PAL-287 (B; $n = 5$), 30 µM PAL-1046 (C; $n = 5$), 30 µM PAL-1045 (D; $n = 5$), 10 µM 5-HT (E; $n = 5$), and 30 µM p-chloroamphetamine (F; $n = 5$). Data are means ± SD. The data points were fitted by monoexponential functions in the case of 5-HT and the PAL substrates. A biexponential function was used to fit the recovery data of p-chloroamphetamine. The insets in B and C show a magnified view of the data points and fits near to the respective time constants, which are indicated by the dashed lines. **(G)** Relaxation rates were obtained by the fits from B–F. The rates shown for p-chloroamphetamine are the k_{fast} values obtained from the biexponential fit. The k_{slow} values are (±SEM) 10 mM Na^+_e: 0.35 ± 0.23 s^{-1}; 70 mM Na^+_e: 0.10 ± 0.12 s^{-1}; 140 mM Na^+_e: 0.49 ± 0.15 s^{-1}. Data are means ± 95% confidence intervals of the fits. The points marked in blue were taken from a previously published study (Bhat et al., 2017). Statistical significance was determined by one-way ANOVA followed by multiple comparisons using the Fisher's LSD method. *, $P < 0.05$; **, $P < 0.01$; ***, $P < 0.001$; ****, $P < 0.0001$; n.s., not significant.
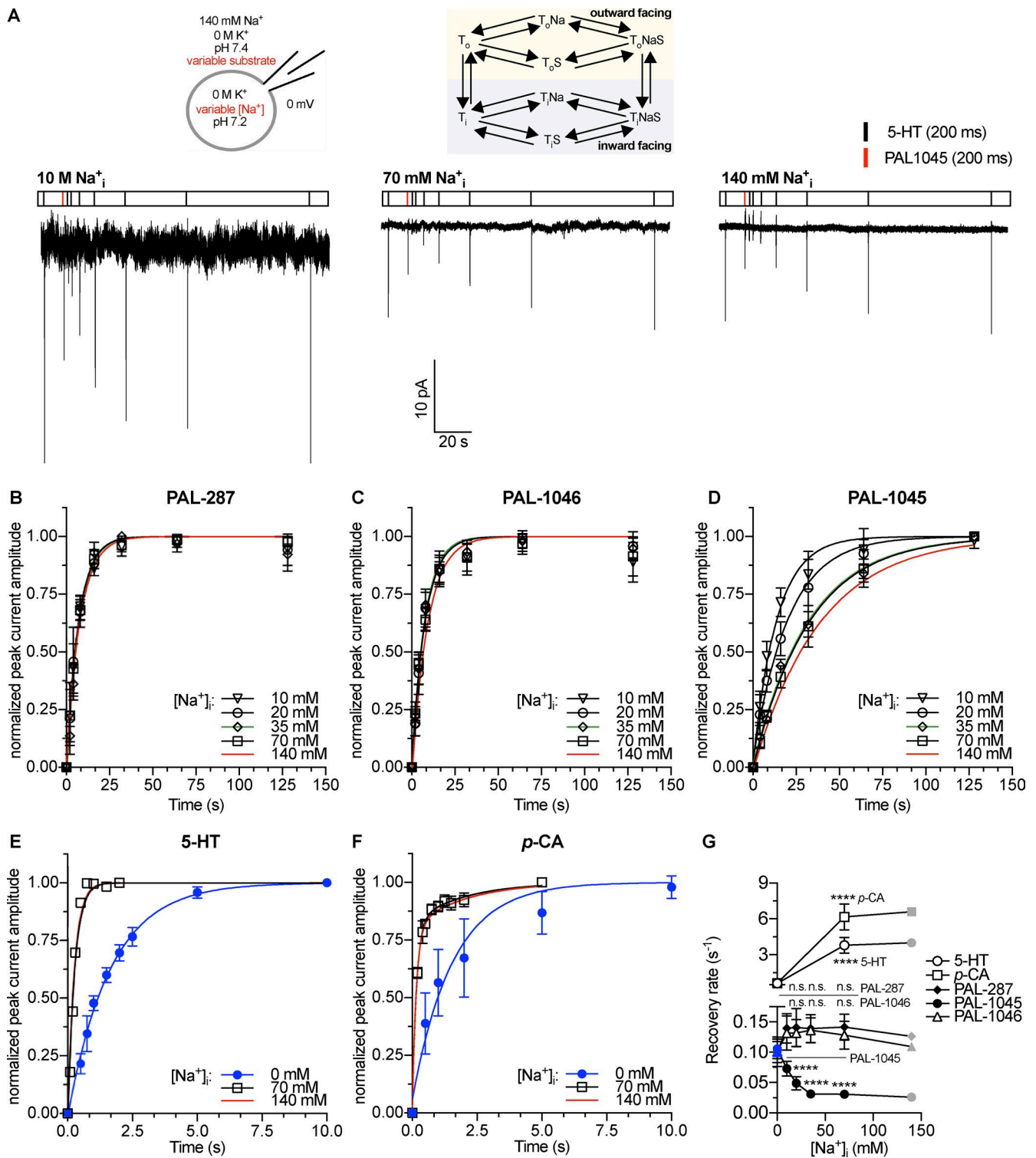
Figure 2. **Peak current recovery as a function of intracellular Na$^+$ concentration. (A)** Top: Schematic rendering of the recording conditions indicating the concentrations of intracellular and extracellular substrate and cosubstrate ions and reaction scheme of a Na$^+$-coupled transporter. Bottom: Original traces of representative experiments using 10, 70, or 140 mM intracellular Na$^+$. **(B–F)** Time-dependent recovery of 5-HT–induced (10 μM) peak current amplitude after application of 30 μM PAL-287 (B; $n = 4$–6), 30 μM PAL-1046 (C; $n = 5$–7), 30 μM PAL-1045 (D; $n = 5$), 10 μM 5-HT (E; $n = 5$), and 30 μM p-chloroamphetamine (F; $n = 5$). The red curves in B–D are the fits of data displayed in Fig. 1. Data are means ± SD. The data points were fitted by monoexponential functions in the case of 5-HT and the PAL substrates. A biexponential function was used to fit the recovery data of p-chloroamphetamine at 70 and 140 mM Na^+_i. For the Na^+_i-free condition, a monoexponential fit was used. **(G)** Relaxation rates were obtained by the fits from B–F. The rates shown for p-chloroamphetamine are the k_{fast} values obtained from the biexponential fit. The k_{slow} values are (±SEM) 70 mM Na^+_i: 0.50 ± 0.11 s^{-1}; 140 mM Na^+_i: 0.49 ± 0.15 s^{-1}. Data are means ± 95% confidence intervals of the fits. The points marked

Cooperative binding of Na$^+$ and substrate to SERT | Hasenhuetl et al.

traces were filtered at 1 kHz and digitized at 2 kHz using a Digidata 1320A (MDS Analytical Technologies). Drugs were applied using a DAD-12 (ALA Scientific Instruments), which allows for rapid solution exchange (Schicker et al., 2012; Hasenhuetl et al., 2016). Current amplitudes in response to 5-HT application were quantified using Clampfit 10.2 software (Molecular Devices). Passive holding currents were subtracted, and the traces were filtered using a 100-Hz digital Gaussian low-pass filter.

Release experiments

Outwardly directed transport flux assays were performed as described previously (Scholze et al., 2000; Mayer et al., 2017). In brief, HEK293 cells expressing human SERT carrying an N-terminal green fluorescent protein tag under the control of a tetracycline-inducible expression system were seeded 24 h before the release assay onto poly-D-lysine–coated glass coverslips (5-mm diameter, 40,000 cells per coverslip). Preloading of the cells with tritiated substrate was ensured by exposing the cells to 0.1 µM [^{3}H]MPP$^+$ for 20 min at 37°C. Subsequently, the cells were transferred into small chambers (total volume of 200 µl) and superfused with K$^+$-free buffer (flow rate of 0.7 ml per min) containing 100 µM ouabain for 40 min to establish a basal release. After 40 min, the collection of 2-min fractions was initiated. After three basal fractions, the cells were exposed to either 10 µM monensin or solvent (ethanol, 96%) for four fractions before 3 µM *p*-chloroamphetamine or PAL1045, respectively, was added for another five fractions. Finally, the cells were superfused with SDS (1%) for three fractions. The total amount of tritium within the superfusates was determined by use of a β-scintillation counter. The amount of [^{3}H]MPP$^+$ released per fraction was expressed as a fractional rate (i.e., the percentage of the total amount of radioactivity present at the beginning of that fraction; Sitte et al., 2000).

Statistics

Experimental variations are either reported as means ± 95% confidence intervals, means ± SD, or means ± SEM.

Peak current recovery data were fitted to the equation describing a monoexponential rise to a maximum. The data generated with *p*-chloroamphetamine were better described by a biexponential rise to a maximum (i.e., the sum of two exponential processes). We attribute the slow component of the recovery to back diffusion of *p*-chloroamphetamine from the cell lumen (Sandtner et al., 2014). This diffusion does not affect recovery rates

in the case of the PAL substrates because of their slow dissociation rates (Figs. 1 and 2; Bhat et al., 2017). Significant differences in peak current recovery rates (Figs. 1 and 2) were determined by one-way ANOVA followed by multiple comparisons using the Fisher's least significant difference (LSD) method. In the case of *p*-choloroamphetamine and 5-HT in Fig. 2, unpaired *t* tests were used. Data from concentration–response curves were fitted to a rectangular hyperbola to obtain estimates for EC_{50} and maximum transport or efflux.

Modeling

The cooperative binding model of SERT was developed based on a published sequential binding model (Schicker et al., 2012; Hasenhuetl et al., 2016). The evolution of state occupancies was computed by numerical integration of the resulting system of differential equations using the Systems Biology Toolbox (Schmidt and Jirstrand, 2006) and MATLAB 2017a software (Mathworks). The voltage dependence of individual partial reactions was modeled according to Läuger (1991) assuming a symmetric barrier as

$$k_{ij} = k^0_{ij}e^{-zQijFV/2RT},$$

where F = 96,485 C·mol^{-1}, R = 8.314 JK^{-1}mol^{-1}, V is the membrane voltage in volts, and T = 293 K. Coupled membrane currents upon application of substrate were calculated as

$$I = -F \times NC/N_A \times \Sigma z_{Qij}(p_i k_{ij} - p_j k_{ji}),$$

where z_{Qij} is the net charge transferred during the transition, NC is the number of transporters (4 × 10^6/cell), and N_A = 6.022e^{23}/mol. The substrate-induced uncoupled current was modeled as a current through a Na$^+$-permeable channel with

$$I = P_c\gamma NC(V - V_{rev}),$$

where P_c corresponds to the occupancy of the channel state, γ is the single-channel conductance of 2.4 pS, NC is the number of transporters (4 × 10^6/cell), V is the membrane voltage, and V_{rev} is the reversal potential of Na$^+$ (80 mV). The extracellular and intracellular ion concentrations were set to the values used in the respective experiments. To account for the noninstantaneous onset of the substrate in patch-clamp experiments, we modeled the substrate application as an exponential rise with a time constant of 10 ms.

in blue were obtained from data published in a previous study (Bhat et al., 2017). The gray points displayed for 140 mM Na^+_i (which equals 140 mM Na^+_e) were taken from Fig. 1 for comparison. Statistical significance was determined by one-way ANOVA followed by multiple comparisons using the Fisher's LSD method or by an unpaired *t* test in the case of 5-HT and *p*-chloroamphetamine. ****, P < 0.0001; n.s., not significant.
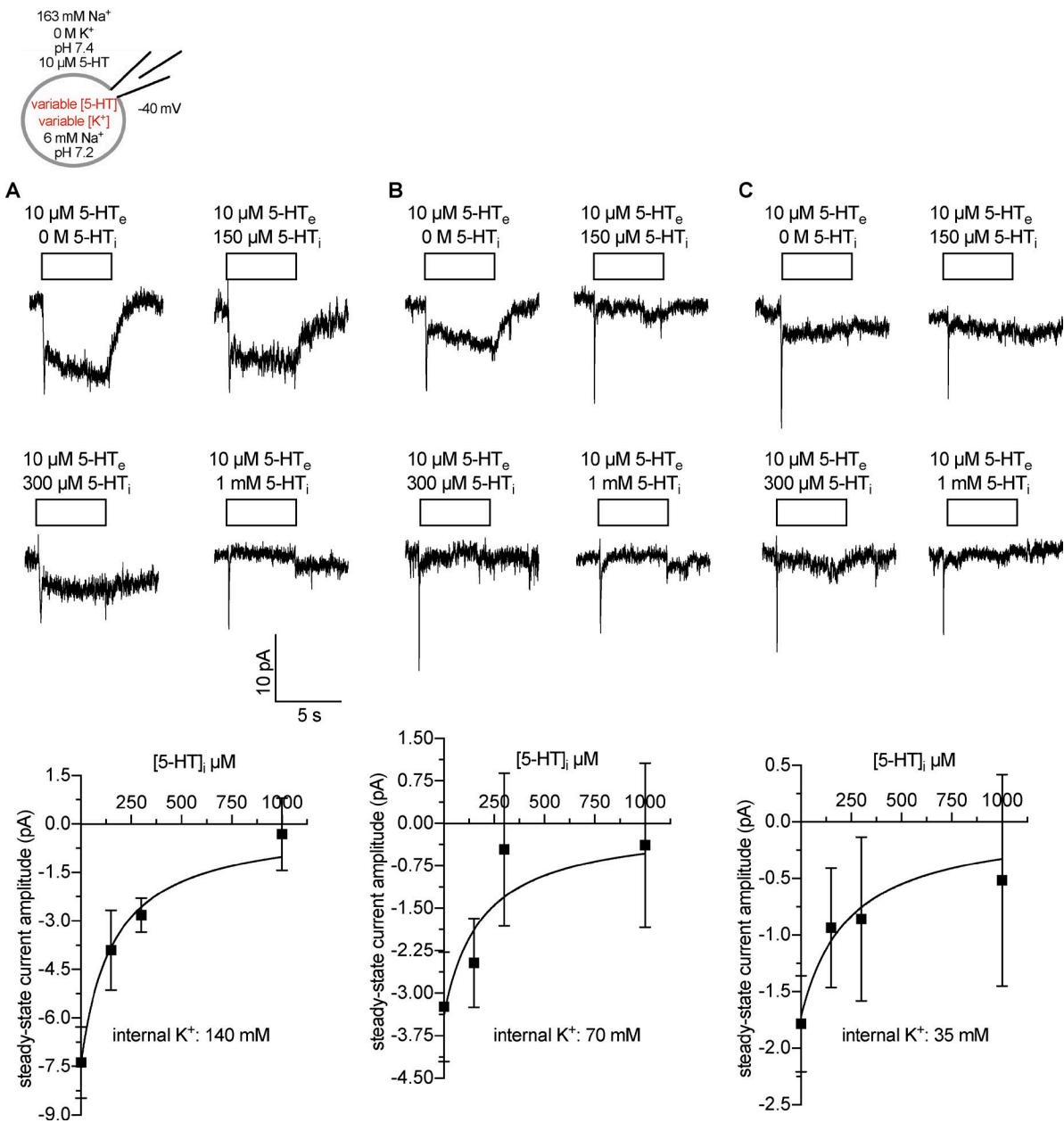
Figure 3. **Internal 5-HT binding as a function of intracellular K$^+$ concentrations.** Scheme: Representation of the recording conditions indicating the concentrations of intracellular and extracellular substrate and cosubstrate ions. **(A–C)** Top: Original traces of representative experiments at intracellular K$^+$ concentrations of 140 (A), 70 (B), and 35 mM (C). Bottom: Corresponding quantification of steady-state current amplitudes induced by 10 µM 5-HT. Data are means ± SD (n = 5–11). The solid lines were drawn by fitting the data to a rectangular hyperbola.

Peak current recovery after substrate application (Figs. 5, A2, and A4) was modeled as the time-dependent return of the system to ToClNa (Fig. 5 A). Substrate release was modeled as time-dependent substrate dissociation from ToClNaS, ToClKS, and ToClS (Fig. 5 A) multiplied by NC and divided by N_A (see above). Conversely, substrate uptake (Fig. A3) was modeled as substrate dissociation from TiClNaS, TiClKS, and TiClS (Fig. 5 A) multiplied by NC and divided by N_A and normalized to the maximal uptake. Displacement of imipramine binding (Fig. A3) was simulated

as substrate concentration–dependent occupancy of an inhibitor-bound state. The inhibitor (rates shown in figure legend) was modeled to bind to ToClNa (not depicted in Fig. 5 A).

RESULTS

We investigated whether cooperative binding provided a unifying explanation for the forward-transport mode of monoamine transporters and the releasing action of amphetamines by addressing the following

Cooperative binding of Na$^+$ and substrate to SERT | Hasenhuetl et al.

questions. (a) Do substrate and Na^+ bind to SERT in a cooperative manner? (b) Does K^+ binding, which promotes forward transport, oppose the effect of Na^+ binding by decreasing substrate affinity? (c) Can a parsimonious cooperative binding model account for the releasing action of amphetamines, or are additional transport modes required? (d) Can the model predict the dependence of substrate release on the intracellular concentration of Na^+ and on the identity of an amphetamine-like congener?

Dependence of substrate dissociation on intracellular and extracellular Na^+ concentration

We tested whether the binding of substrate and of Na^+ to SERT (both extracellularly and intracellularly) was cooperative. We reasoned that the time course over which substrates dissociate from the transporter as a function of intracellular and extracellular Na^+ concentrations should provide insights into the mechanism of interaction between substrate and Na^+. To this end, we recorded SERT-mediated currents in HEK293 cells using whole-cell patch-clamp recordings; these allowed us to control both extracellular (through the bath solution) and intracellular (through the patch pipette) ionic concentrations (see Materials and methods). Currents carried through SERT under physiological ion gradients (high extracellular Na^+ and high intracellular K^+ concentrations) consist of two components (Schicker et al., 2012; Hasenhuetl et al., 2016): (1) an initial and transient peak current, which reflects the movement of substrate and Na^+ through the membrane electric field; its amplitude is proportional to the number of transporters residing in an outward-facing, substrate-free state, and (2) a steady-state current that persists during substrate application; this current requires internal K^+ and is a readout of the forward-transport mode of the transporter. These two currents therefore reflect distinct partial reactions in the transport cycle of SERT and are dependent on the used cosubstrate gradients. Substrate-induced currents through SERT are thus useful signals to track the conformational transitions of this protein with high temporal resolution. We examined the interaction of intracellular and extracellular Na^+ with five different substrates: 5-HT, *p*-chloroamphetamine, and the naphthyl-propan-amines PAL-287, PAL-1045, and PAL-1046 to SERT. The latter three compounds are atypical releasers (Rothman et al., 2012), which have been shown to display slow dissociation kinetics (Bhat et al., 2017). These substrates are thus ideally suited to study the effect of Na^+ on the stability of the substrate–transporter complex. For instance, their slow dissociation rates from the outward-facing conformation should not change with increasing external Na^+ concentrations if a sequential order is assumed; yet, these off-rates are predicted to decrease if substrate and Na^+ binding is cooperative. We investigated the effect of

Na^+ on substrate binding to SERT by relying on external and internal K^+-free solutions, which contained Na^+ concentrations ranging from 10 to 140 mM (see Materials and methods). Depleting intracellular K^+ isolates the peak component of the substrate-induced current by eliminating the steady-state component. In the absence of intracellular K^+, the transporter still operates in the forward-transport mode, albeit at a substantially slower rate (Hasenhuetl et al., 2016; Bhat et al., 2017). Conversely, increasing the intracellular Na^+ concentration supports the substrate-exchange mode (Hasenhuetl et al., 2016). In this mode, the transporter does not complete the catalytic cycle; instead, it returns to the outward-facing conformation loaded with substrate. The recovery of the transporters from a substrate-loaded to a substrate-free species via these distinct transport modes was quantified using a previously described (Erreger et al., 2008; Hasenhuetl et al., 2016; Bhat et al., 2017) peak current recovery protocol (Figs. 1 A and 2 A). In this protocol, substrate binding generates a peak current; its amplitude serves as a reference for the number of transporters available for substrate binding in the recorded cell. Reapplication of the substrate after a defined wash time generates another peak current; the amplitude of this current is contingent on the number of binding sites, which have released their cognate substrate in the interval between original reference pulse and test pulse. Repeated substrate application at increasing wash time intervals tracks the recovery of substrate-binding sites to 100%. At 100% recovery, the amplitudes of the reference peak and the test peak currents are similar, indicating complete dissociation of all substrate molecules occupying the binding sites before application of the test pulse.

Extracellular Na^+. We first tested this recovery as a function of extracellular Na^+ concentrations with a fixed intracellular Na^+ concentration of 140 mM. Fig. 1 A shows current traces from three representative experiments. We applied substrate for 200 ms and tested the recovery of substrate-binding sites by applying 10 µM 5-HT. The amplitude of the 5-HT–induced peak current served as a measure of recovered outward-facing transporters (Hasenhuetl et al., 2016; Bhat et al., 2017). 5-HT was used to probe the recovered binding sites in all cases because PAL-287, PAL-1045, and PAL-1046 require very long washout times between sweeps (up to 2 min for PAL-1045 compared with 10–30 s for 5-HT). The time courses of recovery were fit to monoexponential functions to obtain estimates for the recovery rates in the case of the PAL substrates and 5-HT (Fig. 1, B–E). In the case of *p*-chloroamphetamine, a biexponential function was used because the fit was significantly improved (F test, P < 0.0052). It is evident from Fig. 1 G that the kinetics differed significantly between substrates by up to two orders of magnitude (e.g., 0.025 ± 0.001 s^{-1} for PAL-

1045 vs. 4.012 ± 0.211 s^{-1} for 5-HT). We did not detect any dependence of the recovery rates on extracellular Na$^+$ concentration after 5-HT or p-chloroamphetamine application, which is expected because of their rapid dissociation kinetics. However, in the case of all three PAL substrates, there was a statistically significant ~2.5-fold increase in recovery rates when extracellular Na$^+$ concentrations were reduced from 140 to 10 mM. This observation is incompatible with a sequential binding order but is consistent with cooperative binding of substrate and Na$^+$.

Intracellular Na$^+$. In a second set of experiments, we measured peak current recovery rates at varying intracellular Na$^+$ concentrations but at a fixed extracellular Na$^+$ concentration of 140 mM (Fig. 2, A–F). We found that Na$^+$ had differential effects on these rates (Fig. 2 G). In the case of 5-HT and p-chloroamphetamine, the rates of peak current recovery increased in the tested range of intracellular Na$^+$ concentrations (0 M to 140 mM intracellular Na$^+$) by ~6.7-fold and 10-fold, respectively. These changes in recovery rates have been attributed to the Na$^+$-induced switch of the transporter from the slow forward-transport mode in the absence of intracellular K$^+$ to the rapid substrate-exchange mode in the presence of high intracellular Na$^+$ concentrations (Erreger et al., 2008; Hasenhuetl et al., 2016; Bhat et al., 2017; Kern et al., 2017). When PAL-287 and PAL-1046 were examined, the rates were substantially lower than those obtained with 5-HT and p-chloroamphetamine, but they did not change with Na$^+$ concentration. However, for PAL-1045, the rate of recovery decreased fourfold with increasing Na$^+$ between 0 and 140 mM Na$^+$. These data suggested that the affinity of these substrates increased with Na$^+$ concentrations (more specifically PAL-1045), which suggested cooperative binding. Importantly, individual substrates differed in the extent to which their affinity was modulated by Na$^+$, indicating that the degree of this cooperativity was substrate dependent.

Destabilization of the substrate–transporter complex by K$^+$

It is plausible to posit that, in a cooperative binding mechanism, K$^+$ opposes the action of Na$^+$ and decreases substrate affinity. This possibility is supported by several observations. For instance, under physiological conditions, SERT returns to the outward-facing conformation in a K$^+$-bound form (Nelson and Rudnick, 1979). This reaction is thought to be the rate-limiting step of the transport cycle (Schicker et al., 2012). In the absence of intracellular Na$^+$ and K$^+$, peak current recovery for all three PAL substrates was substantially slower than the corresponding rates obtained with 5-HT and p-chloroamphetamine (Fig. 2; Bhat et al., 2017). These data suggest that dissociation of the PAL substrates from the

inward-facing conformation was rate limiting for the return to the outward-facing conformation. However, physiological intracellular K$^+$ concentrations accelerated internal PAL dissociation by at least 30-fold, such that it was not rate limiting for completion of the transport cycle (Bhat et al., 2017). These findings suggest that K$^+$ binding lowers substrate affinity, which may be achieved in two ways: (1) K$^+$ may reduce the apparent substrate affinity simply by competing with Na$^+$ for binding. This is predicted to shorten the residence time at the inward-facing conformation and to thereby lower the probability for rebinding of intracellular substrate; (2) alternatively, the substrate affinity may be directly reduced by K$^+$ binding (e.g., via an increase of the substrate dissociation rate).

Low apparent affinity of internal 5-HT in the presence of internal K$^+$. We tested these possibilities and first measured the inhibition of steady-state currents by intracellular 5-HT (Adams and DeFelice, 2003; Hasenhuetl et al., 2016) as a function of intracellular K$^+$ concentrations. The steady-state current amplitudes decreased with increasing internal 5-HT concentrations (Fig. 3 A). Consistent with a previous study (Hasenhuetl et al., 2016), an internal 5-HT concentration of 1 mM was necessary to eliminate the steady-state current in the presence of 140 mM internal K$^+$. Half-maximal inhibition of the steady-state current occurred at 158.50 µM (95% CI: 108.90–237.40 µM; $r^2 = 0.84$; Fig. 3 A). This apparent affinity is approximately one order of magnitude lower than the potency of 5-HT to displace [^{3}H]β-CIT from the outward-facing conformation (Korkhov et al., 2006) and three orders of magnitude lower than the potency to induce steady-state currents (Schicker et al., 2012). These data suggest that the ionic composition (high [K$^+$]/low [Na$^+$]) lowers the apparent 5-HT affinity. Hence, decreasing internal K$^+$ concentrations ought to increase the potency of internal 5-HT to inhibit steady-state currents. However, when intracellular K$^+$ concentrations were lowered to 70 and 35 mM, there was a substantial decrease in steady-state current amplitude (Fig. 3, B and C). This precluded a reliable investigation of the effects of K$^+$ on the potency of substrate-induced inhibition of the steady-state current. The unfavorable signal to noise ratio is evident from the parameter estimates (IC$_{50}$ values: 70 mM K$^+$, 186.30 µM [95% CI: 77.97–539.00 µM; $r^2 = 0.46$], 35 mM K$^+$, 233.30 µM [95% CI: 90.96–828.20 µM; $r^2 = 0.31$]; Fig. 3, B and C).

K$^+$ enhances substrate dissociation. Whole-cell patch-clamp recordings allow for rapid (co)substrate exchange only on the extracellular side. Hence, it is not possible to assess substrate binding to the inward-facing conformation via a time-resolved approach. Nevertheless, if K$^+$ facilitates substrate dissociation from in-
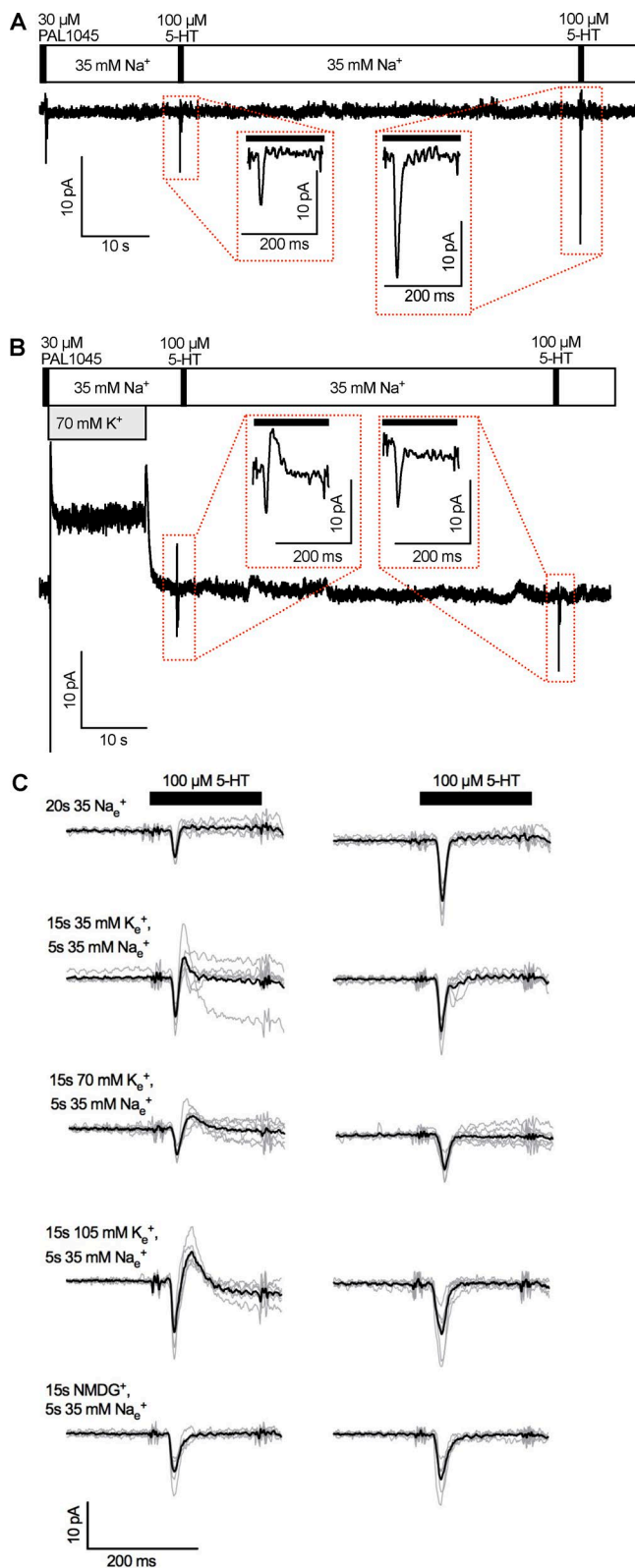
Figure 4. Peak current recovery as a function of extracellular K+ concentrations. (A) Original trace of a representative experiment using a K+-free external solution containing 35 mM Na+. Insets: 5-HT–induced peak currents 20 s (left) and 80 s (right) after application of 30 µM PAL-1045. The black bars indicate the 200-ms 5-HT application. **(B)** Original trace of a represen-

ward-facing transporters, it is plausible that it may also do so at the outward-facing conformation. We therefore resorted to an alternative approach to study the effect of K+ on substrate dissociation and capitalized on the slow dissociation of PAL-1045 ($\sim$0.025 s^{-1}). This slow rate provided a favorable dynamic range for detecting any acceleration of substrate dissociation by K+. We used recording conditions where unbinding of PAL-1045 from the inward-facing conformation was prevented by using an internal solution containing 140 mM Na+. We selected an external Na+ concentration of 35 mM; this concentration was high enough to slow down dissociation of PAL-1045 (Fig. 1, D and G) but was low enough to allow for competition of K+ with Na+ for binding to SERT. The protocol was as follows: we applied 30 µM PAL-1045 for 200 ms and tested the peak current recovery with a pulse of 100 µM 5-HT after 20 s (i.e., after the first half-life of recovery; compare with Fig. 1 D) and after 80 s (the time point where close to 100% recovery was achieved; compare with Fig. 1 D). The initial 20-s wash period after application of PAL-1045 consisted of (a) washing the cell with bath solutions containing 35 mM Na+ and variable K+ concentrations (0, 35, 70, or 105 mM) for 15 s followed by (b) reapplication of the K+-free solution containing 35 mM Na+ for 5 s before the challenge with 100 µM 5-HT. The latter was to avoid two confounding effects: (1) The presence of K+ bound to outward-facing SERT would not allow for peak current induction. It must therefore undergo dissociation. The binding pocket must then be refilled with Na+ before the substrate binds. (2) K+ application to a HEK293 cell is expected to elicit unspecific changes in holding current, which would confound the interpretation of the peak current (compare holding currents of Fig. 4 A without external K+ with Fig. 4 B, where K+ was applied).

Fig. 4 A shows a representative experiment using a K+-free external solution. Although the cell had been washed for 20 s with a solution containing 35 mM Na+, the current after exposure exhibited only half of the amplitude of the control current (compare left vs. right inset in Fig. 4 A). This was consistent with the recovery experiment shown in Fig. 1 D and confirmed slow dissociation of PAL-1045 from SERT at a rate of $\sim$0.025 s^{-1}.

tative experiment using an external solution containing 35 mM Na+ and 70 mM K+. K+ was applied for 15 s after the PAL-1045 pulse. The external Na+ concentration (35 mM) was held constant throughout the recording. Inset: 5-HT–induced peak current after application of 70 mM K+ for 15 s and a wash period of 5 s with 35 mM Na+. Note the outward current component, which was not seen in the absence of prior K+. **(C)** Peak current traces taken from five experiments per experimental condition (the five experimental conditions are indicated on the left). The black traces represent the means of individual traces shown in gray. The black bars indicate the application of 5-HT for 200 ms. The left- and right-hand traces are 5-HT–induced currents 20 s and 80 s after PAL-1045 application, respectively.

Fig. 4 B shows a representative experiment in which PAL-1045 was washed off with a solution containing 70 mM K^+ in addition to 35 mM Na^+. Although K^+ had been removed 5 s before application of 5-HT, the shape of the 5-HT–induced current changed substantially. First, we observed an inwardly directed component, which was the result of substrate binding to the fraction of transporters in the outward-facing conformation. This was followed by an outwardly directed component, which appeared upon current relaxation (Fig. 4 B, left inset). The outwardly directed current is reminiscent of an outward current observed in DAT (Erreger et al., 2008). This current has been associated with the isomerization of the substrate-bound transporter from the inward-facing to the outward-facing conformation; it has therefore been interpreted as the mirror image of the substrate-induced inward peak current. Because substrate translocation is also electrogenic in SERT (Schicker et al., 2012; Hasenhuetl et al., 2016), an outward peak current is the expected consequence of intracellular substrate binding to transporters, which are trapped in the inward-facing conformation. This was likely the case in the present experiment for the following reasons. (a) High extracellular K^+ concentration and high intracellular Na^+ concentration reversed the cosubstrate gradients. These gradients are predicted to shift the conformational equilibrium toward the inward-facing conformation. Additionally, inward-facing transporters are conformationally trapped under high intracellular Na^+ at concentrations four times higher than that seen by transporters in the outward-facing conformation. Thus, as a mirror image of the physiological transport cycle, the following rules apply: The inward-facing transporter can only translocate to the outward-facing conformation either loaded with K^+ or with Na^+ plus substrate. More importantly, the outward-facing K^+-bound transporter can only translocate to the inward-facing conformation once the substrate has dissociated. (b) Extracellular application of 100 µM 5-HT has been shown to result in diffusion of 5-HT into the cell and binding to the inward-facing conformation (Sandtner et al., 2014). Given the present experimental conditions, application of 100 µM 5-HT ought to result in internal binding to the transporter, leading to an outward current.

It is worth noting that K^+ altered the current, although it had been removed 5 s before the application of 5-HT. At this time point, K^+ must have fully dissociated from the transporter (Schicker et al., 2012; Hasenhuetl et al., 2016). In addition, the outward current elicited by 5-HT required complete dissociation of the PAL substrate because sustained binding of PAL-1045 (Bhat et al., 2017) would have precluded the accumulation of transporters in the inward-facing state (as seen in the absence of external K^+; Fig. 4 A). Thus, the data summarized in Fig. 4 B imply that PAL-1045 dissociated from the out-

ward open state before the removal of K^+. The conclusion that K^+ enhances PAL-1045 dissociation—and does not simply compete with Na^+—was further corroborated by experiments that used only NMDG in the wash solution (i.e., no Na^+ or K^+ during the wash phase). These recordings did not reveal any change in the shape or amplitude of the peak current (compare the different experimental conditions in Fig. 4 C). Collectively, the data suggest that K^+ directly decreases substrate affinity. Importantly, this implies that a ternary complex of SERT–substrate–K^+ (in this case, SERT–PAL-1045–K^+) exists and that K^+ and substrate do not bind to SERT in a mutually exclusive manner.

A cooperative binding model of SERT

Currently available transport models implicitly assume or explicitly posit sequential binding of substrates and cosubstrates (Erreger et al., 2008; Schicker et al., 2012; Sandtner et al., 2014; Hasenhuetl et al., 2016), but these cannot account for the observed effect of Na^+ or K^+ binding on substrate affinity. Most importantly, no currently available kinetic model can quantitatively account for amphetamine action. Accordingly, we designed a kinetic model of SERT in which we replaced sequential binding by a random, but cooperative, binding order (Fig. 5 A; and see Appendix). We emphasize that the kinetic parameters were not set to specifically account for amphetamine-induced substrate release. Rather, the parameters were constrained by the findings from the electrophysiological experiments and by data from radioligand binding and uptake inhibition assays to test whether the resulting physiological transport modes would suffice to explain the releasing action of amphetamines. A detailed description of how the kinetic parameters were derived can be found in the Appendix. The central tenet of the model is that cooperative binding unites the features of sequential and random binding and should therefore account for both the physiological function of SERT and the action of amphetamines. It assumes that the affinities of Na^+ and substrate are low when they bind alone, but that their affinities increase upon ternary complex formation. We applied this principle by using cooperativity factor α, which specified the extent to which formation of the ternary complex reduced the dissociation rates of substrate and Na^+. For instance, an α value of 1 (i.e., no cooperativity) does not change the dissociation rates, whereas an α value of 10 would decrease dissociation rates by a factor of 10, thus increasing the affinity 10-fold. The model also allowed cooperativity factor α to differ for individual substrates while maintaining microscopic reversibility.

It is important to note that the cooperative binding model was designed such that it effectively behaves like a sequential binding model when physiological ion gradients are used. The dissociation rate of internal Na^+
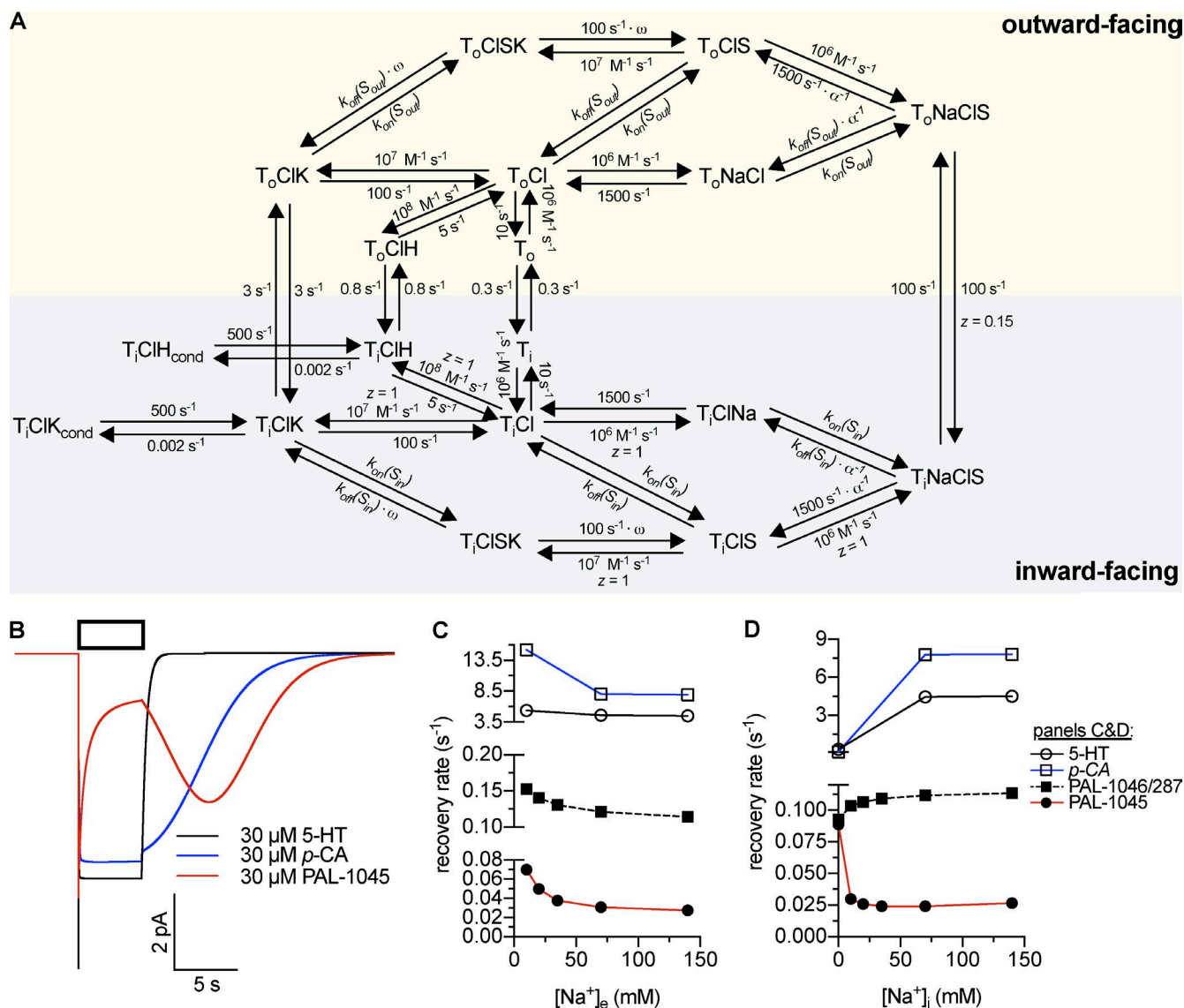
Figure 5. **Cooperative binding model of SERT. (A)** Kinetic scheme of the model. $k_{on}(S_{out}) = 10^7$ M^{-1} s^{-1} (5-HT/PAL-1045/1046/287), 2×10^6 M^{-1} s^{-1} (p-chloroamphetamine); $k_{off}(S_{out}) = 10$ s^{-1} (5-HT, p-chloroamphetamine), 0.5 s^{-1} (PAL-1045), 15 s^{-1} (PAL-1046/287); $k_{on}(S_{in}) = 10^6$ M^{-1} s^{-1} (5-HT/PAL-1046/287), 7×10^7 M^{-1} s^{-1} (PAL-1045), 10^5 M^{-1} s^{-1} (p-chloroamphetamine); $k_{off}(S_{in}) = 1$ s^{-1} (5-HT), 3.5 s^{-1} (PAL-1045), 1.5 s^{-1} (PAL-1046/287), 0.5 s^{-1} (p-chloroamphetamine). α values: 5-HT, 30; PAL-1045, 25; PAL-1046/287, 20; p-chloroamphetamine, 1. ω values: 200 for all substrates. **(B)** Simulated current traces of 30 µM 5-HT, 30 µM PAL-1045, and 30 µM p-chloroamphetamine. This panel reproduces experimental data described in Bhat et al. (2017) and Sandtner et al. (2014). **(C and D)** Simulation of Na$^+$ dependence of peak current recovery at varying extracellular (C) and intracellular (D) Na$^+$ concentrations. This simulation reproduces data shown in Figs. 1 and 2 and partly in Bhat et al. (2017). The time course of recovery after substrate application was modeled as the time course of return to ToClNa after substrate application. For the data points shown for p-chloro-amphetamine, k_{fast} values obtained from the biexponential fits were used (see Materials and methods).

from the ternary complex (1,500 s^{-1} divided by α) is substantially higher than that of substrate (0.5–3.5 s^{-1} divided by α; Fig. 5); Na$^+$ will thus dissociate before the substrate. Yet, it allows for substrate exchange when high internal Na$^+$ concentrations are used.

The cooperative binding model accounts for the experimental observations. Fig. 5 B shows simulated current traces induced by 30 µM 5-HT (black trace), p-chloro-amphetamine (blue trace), and PAL-1045 (red trace). It

is evident that the model accounts for the previously described substrate-induced currents (Bhat et al., 2017). Consistent with experimental observations, the current induced by PAL-1045 decreased in amplitude during the course of substrate application and displayed a biphasic relaxation upon substrate removal (i.e., there was an initial increase in current amplitude followed by a slow decay). This complex signature of amphet-amine-induced currents has previously been explained by diffusion into the cell (because of their lipophilic na-

ture) and internal amphetamine binding to the transporter (Sandtner et al., 2014). In the case of the PAL substrates, this already occurred at lower concentrations than those in the case of *p*-chloroamphetamine (Bhat et al., 2017) and was reproduced by the model. The assumption that PAL substrates display higher affinities to SERT than *p*-chloroamphetamine accounted for the different current profiles. To restrict the complexity of the model to a minimum, we did not use the previously established model for amphetamine diffusion via the cell membrane (Sandtner et al., 2014). Instead, we defined the time-dependent rise in intracellular substrate concentrations as the concomitant inward (and outward) flow of substrate with a time constant of 10 ms. The diffusion of the amphetamines into the cell was required to model the bell-shaped concentration dependence of amphetamine-induced substrate release (Fig. 6 C).

We examined whether the dependence of tested substrates on intracellular and extracellular Na$^+$ concentrations was accounted for by cooperative binding by simulating the peak current recovery experiment using the same conditions as those presented in Figs. 1 and 2. It is evident from Fig. 5 (C and D) that the model recapitulated the recovery rates of 5-HT, *p*-chloroamphetamine, and the PAL substrates as a function of internal and external Na$^+$ concentrations. The kinetic rates used to model the binding of the PAL substrates also allowed for simulating their affinities determined in radioligand binding experiments (see Appendix; Bhat et al., 2017). Analogous to Na$^+$ binding, we used a negative cooperativity factor ω for K$^+$ binding (Fig. 5 A). This factor determined the extent to which K$^+$ binding decreased substrate affinity and vice versa. For the sake of simplicity, H$^+$ was modeled to bind in a sequential order, although we suspect that H$^+$ ions bind in a similar fashion as K$^+$.

A kinetic account for amphetamine-induced monoamine release. The main reason to introduce a cooperative binding model was to examine whether an alternating access model is sufficient to account quantitatively for amphetamine-induced monoamine release, or whether additional amphetamine-specific modes (such as a substrate-conducting pore) were required. We therefore simulated 5-HT release upon application of external *p*-chloroamphetamine. As shown in Fig. 6 A, the model captured increased 5-HT release with increasing intracellular Na$^+$ concentrations, which is a feature that cannot be explained by a sequential binding model. The EC_{50} value of *p*-chloroamphetamine to induce 5-HT release was ~3 µM. It therefore matched the experimentally determined value (Hilber et al., 2005; Seidel et al., 2005). In addition, the calculated rate of *p*-chloroamphetamine–induced 5-HT release was in agreement with experimental data; the maximal release of 2×10^{-15}

mol 5-HT within the 1-min simulation is equivalent to 2,000 pmol/10^6 cells per minute (Hilber et al., 2005). Thus, the present kinetic model provides, to the best of our knowledge, the first qualitative and quantitative account for amphetamine-induced monoamine release.

A mechanistic explanation for partial release. The efficacy of amphetamine-induced monoamine release varies among substrates; in analogy to the partial agonists of receptors, substrates that display reduced V_{max} values in inducing monoamine efflux have been referred to as partial releasers (Rothman et al., 2012). We propose that at least two mechanisms can account for partial release: First, a substrate may be less efficacious in inducing monoamine release because it binds in distinct modes to the outward-facing conformation. It has been suggested that a methylated derivative of 3,4-methylenedioxy-*N*-methylamphetamine, the partial releaser 3,4-methylenedioxy-*N,N*-dimethylamphetamine (MDDMA), has ~50% of its binding events as a substrate. Alternatively, it can also bind in an inverted orientation as an inhibitor (Sandtner et al., 2016). As shown in Fig. 6 B, substrate efflux induced by MDDMA can be accounted for by assuming that 50% of the compound bound as an inhibitor with the same binding kinetics as the substrate. In the second scenario for partial release, high affinity of the releaser may preclude sufficient exchange between releaser and internal substrate because the releaser displays a long dwell time at the transporter. This is likely the case for the partial releaser PAL-1045 (as shown in Fig. 6 C), which displays the highest affinity of the tested substrates. For PAL-1045, the model predicts a bell-shaped concentration–response curve for release, which is reminiscent of the currents induced by it (Bhat et al., 2017). Note that the potency to induce release differs between the two partial releasers (and *p*-chloroamphetamine): MDDMA is a low-affinity, low-efficacy releaser displaying EC_{50} values of 1–3 µM (depending on the intracellular Na$^+$ concentration; Fig. 6 D); PAL-1045, however, is a high-affinity, low-efficacy releaser with EC_{50} values of ~150–330 nM (Fig. 6 D). The difference in V_{max} values for release among the substrates was dependent on internal Na$^+$ concentrations; it became apparent only at Na$^+$ concentrations of ≥10 mM (compare open circles and squares with open triangles and closed symbols in Fig. 6, A–C and E). However, the EC_{50} values doubled in the case of the full releaser and the partial releasers, though their cooperativity factors differed by a factor of 25 (*p*-chloroamphetamine and MDDMA: random [α value = 1]; PAL-1045: cooperative [α value = 25]; Fig. 6 D). Amphetamine-induced dopamine release increases with membrane potential (Khoshbouei et al., 2003; Kahlig et al., 2005); in addition, intracellular Na$^+$ binding to SERT is highly voltage dependent (Hasenhuetl et al., 2016). We incorporated this voltage dependence into
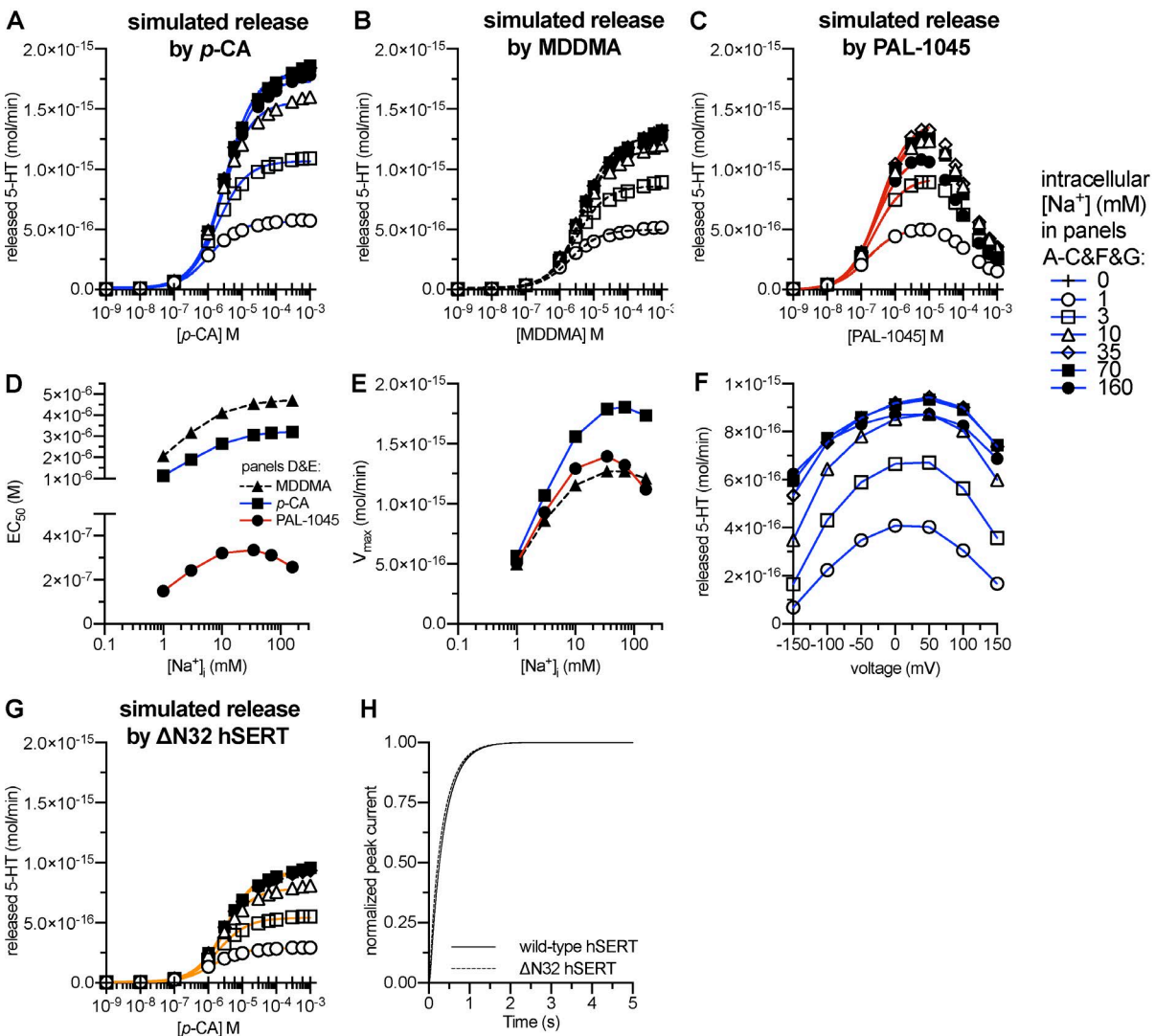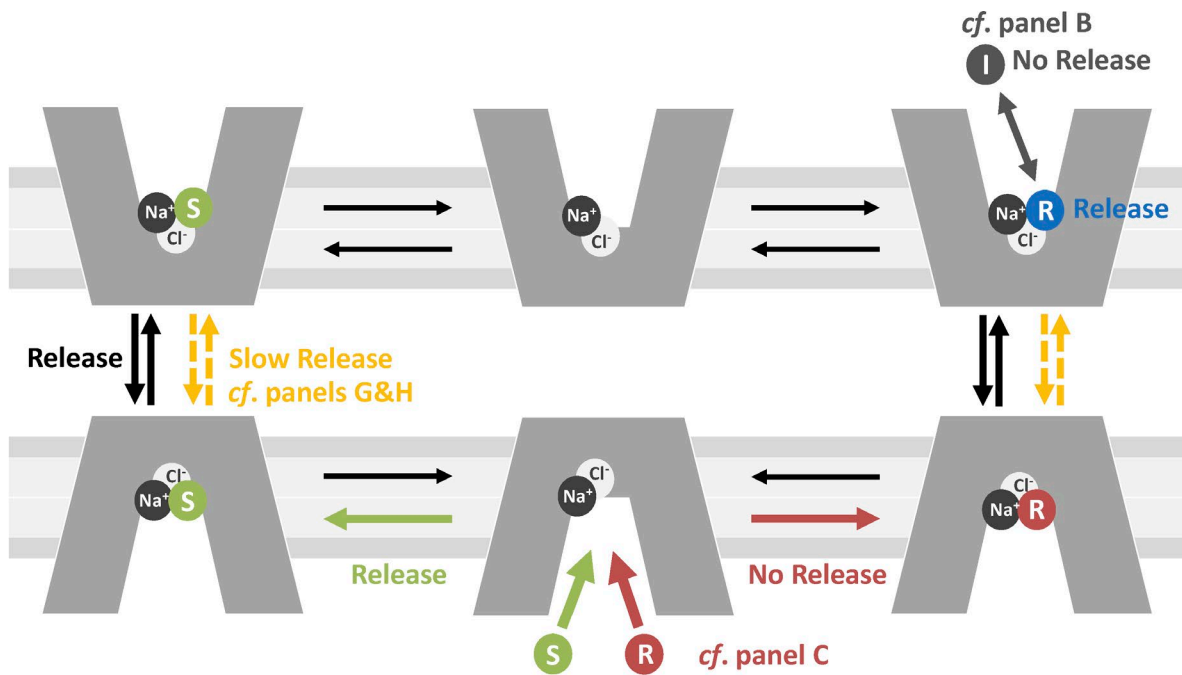
the model (Fig. 5 A and Appendix). When we simulated 5-HT release at 3 µM p-chloroamphetamine at different voltages, we found an increase with membrane potential up to 50 mV. At higher voltages, we observed a decrease in 5-HT release (Fig. 6 F); this bell-shaped relationship has been observed experimentally in DAT (Kahlig et al., 2005).

Truncation of the N terminus of the transporter or its tethering (Sucic et al., 2010; Kern et al., 2017), depletion of membrane lipids (Buchmayer et al., 2013) and the concomitant redistribution of the transporter in membrane microdomains (Cremona et al., 2011; Pizzo et al., 2013), and inhibition of kinase-dependent phosphorylation of the transporter (Fog et al., 2006; Steinkellner et al., 2012, 2014, 2015; Moritz et al., 2015) suppress the reverse transport mode (i.e., they do not impair substrate uptake but they blunt or eliminate amphetamine-induced release). The transport cycle of the mutant hSERT-ΔN32, for instance, has been subjected to a detailed kinetic analysis to understand the role of the N terminus of hSERT in inducing the kinetic switch between the forward-transport (i.e., uptake) and substrate-exchange (i.e., release) modes (Kern et al., 2017). We simulated amphetamine-induced 5-HT release via hSERT-ΔN32 by reducing the transition rate of the substrate-loaded transporter between the inward- and outward-facing conformations (and vice versa; see reaction scheme in Fig. 6) from 100 to 8 s^{-1}. The simulations yielded reduced 5-HT efflux (Fig. 6 G), but a normal turnover rate (Fig. 6 H); i.e., the simulations recapitulated the original experimental observations (Kern et al., 2017).

Assessing substrate release by p-chloroamphetamine and PAL-1045

Our model predicts a major difference in the Na$^+$ dependence of the full releaser p-chloroamphetamine and of the partial releaser PAL-1045 (Fig. 6 E). We tested this prediction in HEK293 cells stably expressing SERT, which had been preloaded with [^{3}H]MPP$^+$. Because of its fixed charge, MPP$^+$ does not permeate the cell membrane, and thus there is no confounding effect caused by background diffusion. The preloaded cells were superfused with buffer containing 100 µM ouabain starting 40 min before the application of the releasing compounds and throughout the experiment (see scheme in Fig. 7 A). Under these conditions, the internal Na$^+$ concentration is expected to rise from ∼3 to ∼10 mM (Harootunian et al., 1989). 2-min fractions of the superfusate were collected. The superfusion with ouabain did not cause any appreciable change in background release resulting in a straight baseline; this can be seen from the six 2-min fractions from 0 to 12 min in Fig. 7 A (the first 28 min of the superfusion with ouabain were omitted in Fig. 7 A). Addition of p-chloroamphetamine (Fig. 7 A, squares) caused a substantially larger release of [^{3}H]MPP$^+$ than PAL-1045 (Fig. 7 A, diamonds). This is consistent with the characterization of PAL-1045 as a partial releaser (Rothman et al., 2012). In Fig. 7 B, we show the calculated release rates in femtomole/minute/cell. These compare favorably with the rates predicted by the model (Fig. 6 E). In parallel, we exposed the cells to 10 µM monensin 10 min before the application of the releasers because this manipulation was predicted to raise the intracellular Na$^+$ concentration by an additional 5 mM (Gildea et al., 2015). The synthetic data in Fig. 6 E predict that this additional increase in internal Na$^+$ ought to enhance the releasing action of p-chloroamphetamine but not of PAL-1045. This prediction of the model was verified by the experimental observations; in the presence of monensin, p-chloroamphetamine caused a significantly larger efflux of [^{3}H]MPP$^+$ release (Fig. 7 A, circles and squares; Fig. 7 B, left bars). In contrast, efflux triggered by PAL-1045 was comparable in the absence and presence of monensin (Fig. 7 A, diamonds and triangles; Fig. 7 B, right bars).

Figure 6. **Simulation of amphetamine-induced serotonin release and partial release.** Top: Schematic rendering of the steps involved in facilitated exchange diffusion. The releaser (R) binds to the outward-facing conformation, leading to isomerization of the transporter to the inward-facing conformation. Upon dissociation of the releaser, the internal substrate binds and can be released after the return of the transporter to the outward-facing conformation. Gray, red, and yellow reactions illustrate the mechanisms of partial release. Gray: A partial releaser may bind in two distinct modes, either as inhibitor (I, in gray) or releaser (R, in blue; see B). Red versus green: A partial releaser may display high affinity to the transporter; this results in a longer dwell time of the releaser in the binding site and thus less exchange between releaser and intracellular monoamine (see C). Yellow: Experimental manipulations may reduce the transition rate between the substrate-loaded outward- and inward-facing conformations; this results in reduced release (see G and H). **(A–C)** Simulation of 5-HT release by increasing concentrations of p-chloroamphetamine (A), MDDMA (B), or PAL-1045 (C) at different intracellular Na$^+$ concentrations. The solid lines were generated by fitting the synthetic data to a rectangular hyperbola to extract EC_{50} values and maximum release (V_{max}). **(D and E)** EC_{50} values (D) and V_{max} values (E) of p-chloroamphetamine, MDDMA, and PAL-1045 in inducing 5-HT release as a function of the intracellular Na$^+$ concentration. **(F)** Voltage dependence of 5-HT release upon application of 3 µM p-chloroamphetamine (approximately the EC_{50}). The release simulations were performed as in A–E, but at voltages ranging from −150 to 150 mV. **(G)** Simulation of 5-HT release by p-chloroamphetamine via the N-terminal mutant hSERT-ΔN32. Simulation conditions were the same as in A–F. **(H)** Turnover rate of N-terminal mutant hSERT-ΔN32 compared with wild-type hSERT. The time course of recovery after substrate application was modeled as the time course of return to ToClNa after 5-HT application.
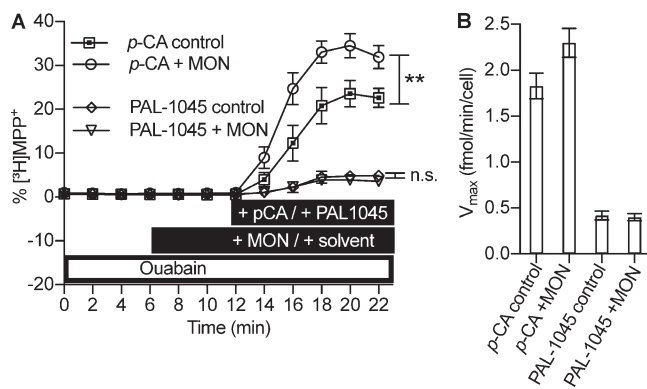
Cooperative binding of Na$^+$ and substrate to SERT | Hasenhuetl et al.

Figure 7. **Substrate release by *p*-chloroamphetamine and PAL-1045. (A)** Release of [³H]MPP⁺ from preloaded HEK293 cells expressing SERT. [³H]MPP⁺ release is plotted as percent [³H]MPP⁺ over time. The experimental conditions are indicated in the black bars: 3 µM *p*-chloroamphetamine (open squares), 3 µM *p*-chloroamphetamine + 10 µM monensin (open circles), 3 µM PAL-1045 (open diamonds), and 3 µM PAL-1045 + 10 µM monensin (open triangles). 100 µM ouabain (open bar) was present starting at t = −40 min and throughout the experiment. For statistical analysis, the total area under the curve after basal release (i.e., fractions t = 0 to t = 4 min) was calculated for each individual trace. **, P < 0.01; n.s., not significant. One-way ANOVA followed by Bonferroni's multiple comparison test. **(B)** Calculated [³H]MPP⁺ release rate for one cell in femtomole/minute (=V_{max}). (A and B) Data are means ± SD, n = 8–9 independent observations per condition.

DISCUSSION

Amphetamines are known to induce the efflux of neurotransmitters via the plasmalemmal monoamine transporters. However, it has remained enigmatic whether they accomplish this by exploiting transport intermediate states, which exist under physiological conditions, or if additional, amphetamine-specific, conformational states are required (Rodriguez-Menchaca et al., 2012). The key conclusion of the present work is that additional transport mechanisms need not be invoked for a mechanistic explanation of amphetamine-induced monoamine release; the action of amphetamine is parsimoniously accounted for by the venerable alternating access model, provided that there is cooperative binding of substrate and cosubstrate. This conclusion is based on the following results: (a) Na⁺ increases substrate affinity, and the extent of this increase depends on the nature of the substrate (Figs. 1 and 2). (b) In addition to positive cooperativity between Na⁺ and substrate binding, we show that K⁺, which selects the forward-transport over the substrate-exchange mode, accelerates substrate dissociation (Fig. 4). (c) A cooperative binding model, which only relies on physiological transport modes, can be derived from the present results and a diverse set of published electrophysiological and biochemical data. This model is, to the best of our knowledge, the first to account qualitatively and quan-

titatively for amphetamine-induced monoamine release (Figs. 5 and 6). (d) The results described in Figs. 1 and 2 and subsequent simulations led to a prediction, which was directly verified in superfusion experiments: increasing the intracellular Na⁺ concentration enhanced amphetamine-induced substrate release in the case of *p*-chloroamphetamine, but not PAL-1045.

We relied on whole-cell patch-clamp electrophysiology to verify that SERT bound Na⁺ and substrate in a cooperative fashion. We tested cooperative binding between substrate and Na⁺ for the three high-affinity naphthyl-propan-amines PAL-287, PAL-1045, and PAL-1046. A sequential binding order, which assumes that substrate dissociation from outward open SERT precedes Na⁺ dissociation, predicts that a variation in extracellular Na⁺ does not have any effect on substrate dissociation. Our experimental results show that this is not the case. Hence, they refute a sequential binding order (Fig. 1). Rather, the present data and previous experiments (Humphreys et al., 1994; Bhat et al., 2017) support the conjecture that Na⁺ increases the affinity of substrate and, importantly, that this effect depends on the nature of the substrate and on the side of titration (intracellular vs. extracellular Na⁺; Figs. 1 and 2). This is indicative of a random but cooperative binding order of substrate and Na⁺. At the current state, it is not possible to design experiments to address which of the two sodium ions binds cooperatively. Based on molecular dynamics simulations, Na⁺ bound to the Na2 site seems to be the logical candidate (Razavi et al., 2017).

A notable feature of cooperative substrate and cosubstrate binding is that it allows for direct competition between Na⁺ and K⁺ (Fig. 5 A), further corroborating the concept that mutually exclusive binding of these cations defines the kinetic decision point between the forward-transport and the substrate-exchange mode (Hasenhuetl et al., 2016). We tested whether K⁺ binding accelerated substrate dissociation. In previous experiments, it was not possible to directly test substrate dissociation because of its rapid kinetics (Schicker et al., 2012). However, the availability of the PAL series of substrates allowed us to overcome this obstacle (Bhat et al., 2017); the slow kinetics of PAL-1045 (∼0.025 s⁻¹), in particular, provided an ideal dynamic range for identifying an interaction between substrate and K⁺. The experiment described here showed that K⁺ binding reduced substrate affinity for SERT (Fig. 4). Although we observed this effect at the outward-facing conformation, we infer that K⁺ also decreases substrate affinity at the inward-facing conformation. This inference is supported by the following experimental observations: (a) The PAL substrates showed equilibrium binding affinity in the nanomolar range when a K⁺-free solution with a high Na⁺ concentration was used. However, they displayed micromolar potency to inhibit substrate uptake (i.e., in the presence of high internal K⁺ concen-

trations). For instance, PAL-1045 displayed a 1,000-fold difference, as it showed a binding affinity of 4 nM but half-maximal uptake inhibition at 4 μM (Bhat et al., 2017). In the simulations, negative cooperativity between K^+ and substrate was required to account for this discrepancy (see Appendix). (b) Dissociation of the PAL substrates from the inward-facing conformation is rate limiting for transporter turnover in the nominal absence of internal K^+ and Na^+; the dissociation rate further decreased with internal Na^+ concentrations (Figs. 1 and 2). However, in the presence of internal K^+, their internal dissociation rates became indistinguishable from those of 5-HT and p-chloroamphetamine (Bhat et al., 2017). (c) K^+ increased the dissociation rate of $[^{125}I]$ β-CIT (the binding site of which likely overlaps with the 5-HT–binding site) to a larger extent than a Na^+-free solution (choline chloride; Korkhov et al., 2006).

Furthermore, recent studies on LeuT indicated that K^+ or H^+ compete with Na^+ (Billesbølle et al., 2016; Khelashvili et al., 2016), and molecular dynamics simulations on a homology model of hDAT suggested that a protonation of the conserved aspartate residue critical for substrate binding (D79 in hDAT and D98 in hSERT) facilitates dissociation of dopamine from the inward-facing conformation (Cheng and Bahar, 2015). A ternary complex model predicts reciprocity of cooperative binding (i.e., substrate also increases Na^+ affinity and decreases K^+ affinity). It has been shown for several transporters, including LeuT, which is the bacterial homologue of the monoamine transporters (Kristensen et al., 2011), that the binding affinities between the ion and substrate are codependent and that this dependence can vary among substrates (Menaker et al., 2006; Tao and Grewer, 2007; Noskov and Roux, 2008).

Most importantly, we show that a cooperative binding scheme is necessary to explain the actions of amphetamines on the monoamine transporters; amphetamine-induced dopamine release has been shown to increase with intracellular Na^+ concentrations (Khoshbouei et al., 2003; Kahlig et al., 2005). This observation cannot be explained by a sequential binding model. If sodium and substrate were bound and released in a sequential order, high intracellular Na^+ concentrations would impede the dissociation of substrate from the inward-facing conformation, thus precluding exchange of internal 5-HT for inwardly transported amphetamine; an alternative explanation invoked the formation of a substrate-conducting pore in response to amphetamine (Kahlig et al., 2005). Although we cannot rule out the possibility that such a pore may occasionally be formed, we emphasize that our ability to account quantitatively for the experimentally observed release rates raises serious doubts about whether such a pore does indeed exist. The substrate-exchange mode is a property of any transporter

that operates via alternating access. In contrast, the formation of a substrate pore is unrelated to the normal operating mode of transporters, which translocate substrates by undergoing a conformational cycle of alternating access. Thus, by definition, positing a substrate pore is not a parsimonious explanation because it is contingent on a major conformational change in the structure of the transporter. In contrast, our cooperative binding model does not require any deviation from the operating mode of a transporter. In fact, it is compatible with the available structural information and all known conformational states, which are visited during the transport cycle. Most of these are accessible by electrophysiological recordings (Hasenhuetl et al., 2016; Bhat et al., 2017; Kern et al., 2017). We tested the cooperative binding model extensively in simulations; the resulting synthetic data recapitulated the experimental observations, regardless of whether they were obtained by electrophysiological recordings, by cellular uptake experiments or in radioligand binding experiments (Hasenhuetl et al., 2016; Bhat et al., 2017; Kern et al., 2017). Therefore, a cooperative binding model, which is based exclusively on the physiological transport modes of SERT, is necessary and sufficient to reproduce the actions of amphetamines. Our experimental approach and consequently developed model are, however, unequipped for assessing entry and exit from intermediate states such as the substrate-loaded occluded state because these are currently not accessible to time-resolved kinetic analysis.

It has remained unclear how structural modifications (Sucic et al., 2010; Kern et al., 2017), phosphorylation/dephosphorylation (Fog et al., 2006; Steinkellner et al., 2012, 2014, 2015), palmitoylation (Moritz et al., 2015), lipid binding (Buchmayer et al., 2013), or association with proteins (e.g., flotillin; Cremona et al., 2011; Pizzo et al., 2013) can have a profound impact on amphetamine-induced release without impinging on the forward-transport mode. This discrepancy is also observed in vivo; the behavioral effects of amphetamines are blunted by disrupting the phosphorylation of DAT or its interaction with flotillin1 in *Drosophila melanogaster* larvae (Pizzo et al., 2013), or by reducing phosphatidylinositol-4,5-bisphosphate binding in adult *D. melanogaster* (Hamilton et al., 2014). However, these manipulations do not affect behavioral readouts for the forward-transport mode (i.e., basal locomotion; Hamilton et al., 2014) and the stimulatory action of the competitive DAT inhibitor methylphenidate (Pizzo et al., 2013). It is currently not known how substrate release, but not uptake, can be selectively affected without violating the rules of microscopic reversibility. In addition, amphetamines were identified that display a reduced efficacy to induce monoamine release when compared with prototypical amphetamines. The cooperative binding

model not only accounted for the releasing action of amphetamines, but it also provided explanations for how these phenomena occur (Fig. 6).

APPENDIX

The kinetic model described here builds on previous models of DAT (Erreger et al., 2008) and SERT (Bulling et al., 2012; Schicker et al., 2012; Sandtner et al., 2014; Hasenhuetl et al., 2016) with the important difference that it is the first to account for amphetamine-induced monoamine release. The kinetic parameters (Fig. 5 A) were derived from a series of electrophysiological, radioligand binding and uptake inhibition experiments. To reduce the complexity of the model, we used symmetric affinities for all substrates and cosubstrates at the outward- and inward-facing conformation and symmetrical transition rates between inward- and outward-facing states. Experimentally observed asymmetry, such as a lower apparent substrate affinity at the inward-facing conformation than at the outward-facing conformation, is a direct consequence of the cooperative binding mechanism (Na^+ increases and K^+ decreases substrate affinity, respectively). Note, however, that affinities of individual (co)substrates need not necessarily be symmetric (Zhao et al., 2010) as long as microscopic reversibility is maintained.

The parameters used in the model were derived from the experiments that follow.

Isomerization between inward- and outward-facing conformations

The substrate-loaded form. The isomerization of the substrate-loaded outward-facing state to the substrate-loaded inward-facing state ($100\ s^{-1}$) was directly measured (see Fig. 4 in Hasenhuetl et al., 2016) and has been shown to be indistinguishable for all five substrates used in this study (see Fig. 3 in Bhat et al., 2017). We assigned this reaction a valence of 0.15 because it sufficiently recapitulated the voltage dependence of the transient peak current when a saturating internal Na^+ concentration was used (see Figs. 3 A and 9 F(ii) in Hasenhuetl et al., 2016).

The substrate-free K^+-bound, substrate-free H^+-bound, and substrate-free empty forms. The return rates of the substrate-free transporter in a K^+-bound, H^+-bound, or empty form were directly measured and are shown in Fig. 6 in Bulling et al. (2012), Figs. 1 and 5–8 in Hasenhuetl et al. (2016), Figs. 5 and 6 in Bhat et al. (2017), and in experiments shown in Figs. 1 and 2 of this paper. The return of the substrate-free transporter to the outward-facing conformation is the rate-limiting reaction for the forward-transport mode and is voltage independent (Mager et al., 1994; Hasenhuetl et al., 2016). Accordingly, we did not assign any valence to this reaction, but to the intracellular binding reactions of Na^+, K^+, and H^+ (which will be described below).

Conducting state

The conducting state ($TiClK_{cond}$ or $TiClH_{cond}$ in Fig. 5 A) of SERT is thought to be a Na^+-conducting pore that is occasionally formed during the transport process. The parameters used to model this state are based on single-channel recordings by Lin et al. (1996), who reported channel lifetimes of ∼2–2.5 ms. This is incorporated in the model by the reaction from the open channel ($TiClK_{cond}$ or $TiClH_{cond}$) to the closed channel ($TiClK$ or $TiClH$) at a rate of $500\ s^{-1}$. Lin et al. (1996) calculated that the conducting state is occupied much less frequently than would be expected if it occurred during every transport cycle. The authors estimated that the open probability (P_o) of the conducting state is $<10^{-6}$. In the model, we set the transition rate from the closed channel ($TiClK$ or $TiClH$) to the open channel ($TiClK_{cond}$ or $TiClH_{cond}$) as $0.002\ s^{-1}$ to account for the reported P_o. The single-channel conductance of 2.4 pS used in the model was also adopted from Lin et al. (1996). The conducting state was modeled to be in equilibrium with a K^+- or H^+-bound inward-facing conformation because the steady-state current was eliminated when internal K^+ was omitted (Schicker et al., 2012; Hasenhuetl et al., 2016) but could be restored if internal H^+ concentrations were raised to a pH of 5.5 (from pH 7.2; Hasenhuetl et al., 2016).

Substrate binding

The association rate constants of all five substrates to the outward-facing conformation have been directly measured by electrophysiological recordings (see Fig. 3 in Bhat et al., 2017) and were incorporated in the model. The dissociation rates and α values (cooperativity factors) were constrained by experiments described in Figs. 1 and 2 of this paper and, in part, in Fig. 5 D in Bhat et al. (2017).

Cation binding

The rates of internal and external cation binding were inferred from a series of electrophysiological experiments (Figs. 1, 2, 3, and 4; Hasenhuetl et al., 2016; Bhat et al., 2017). Although direct measurements of cation-binding rates at the inward- and outward-facing conformation have not yet been possible, these experiments highly constrained the parameter space. Intracellular binding of the three cations Na^+, K^+, and H^+ was assigned a valence of 1 because previous experiments showed that these reactions are highly voltage dependent (Hasenhuetl et al., 2016). The cooperative binding model reproduced the corresponding electrophysiological data; the voltage dependence of the peak current decreased with intracellular Na^+ or K^+ concentrations (Fig. A1; see Fig. 3 in Hasenhuetl et al., 2016).
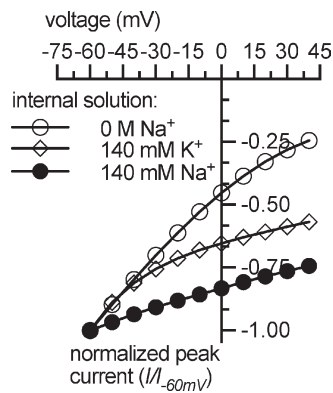
Figure A1. **Simulated current–voltage relationship of 5-HT–induced (10 µM) peak current.** Internal solutions containing (a) 0 M Na^+/K^+, (b) 0 M Na^+/140 mM K^+, and (c) 0 M K^+/140 mM Na^+ were used. The simulations reproduce experimental data described in Hasenhuetl et al. (2016).

Na^+ binding. In the model, Na^+ binding must display a rapid dissociation rate (>100 s^{-1}) because internal Na^+ dissociation has been shown to carry the majority of the charge associated with the substrate-induced peak current (Hasenhuetl et al., 2016). However, the affinity must be sufficiently high to support stabilization of the outward-facing state by high external Na^+ concentrations. Importantly, the increase of peak current recovery rates after 5-HT application by high internal Na^+ concentrations could be simulated by both sequential binding (Hasenhuetl et al., 2016) and cooperative binding (Fig. A2 A), but not by a purely random binding order (Fig. A2 B).

K^+ binding. There are two major constraints on the rates of K^+ binding in the model: (1) K^+ must dissociate rapidly from the outward-facing conformation to not be rate limiting for the forward-transport mode. (2) K^+ must bind the inward-facing conformation rapidly to cancel out the electrogenicity of internal Na^+ dissociation (Fig. A1; Fig. 3 in Hasenhuetl et al., 2016). Support for negative cooperativity of K^+ binding in addition to the data shown in Fig. 4 comes from the observation that the PAL substrates display micromolar potency to inhibit substrate uptake (a condition of high internal K^+ concentrations) but displace the competitive inhibitor imipramine with nanomolar potency (a condition of high Na^+ concentrations on both sides of the membrane; Bhat et al., 2017). This discrepancy could only be accounted for by negative cooperativity and was not observed using a random order (Fig. A3, A and B). In addition, a purely random order of K^+ binding (i.e., an ω value of 1) did not recapitulate the low potency of internal 5-HT to inhibit the steady-state current (Fig. A3 C).

H^+ binding. It has been shown that H^+ ions can functionally replace K^+ in supporting uptake and the steady-state
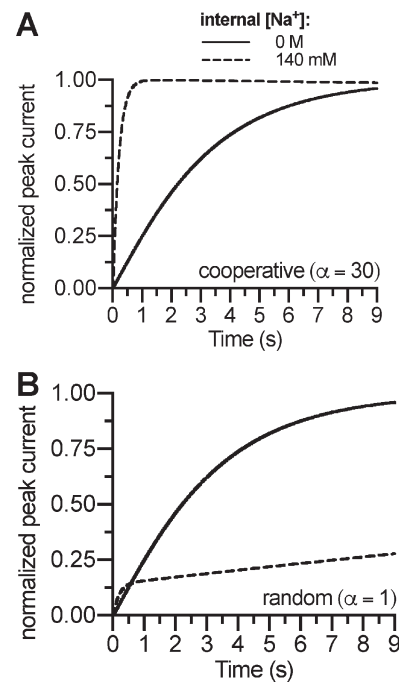

Figure A2. **Induction of the substrate-exchange mode requires cooperative binding. (A)** Simulated peak current recovery experiment using intracellular Na^+ concentrations of 0 M or 140 mM using a cooperativity factor of 30. The time course of recovery after substrate application was modeled as the time course of return to ToClNa (Fig. 5 A). **(B)** Simulated peak current recovery experiment using intracellular Na^+ concentrations of 0 M or 140 mM, but with a cooperativity factor of 1 (i.e., purely random order). The dashed curve reached steady state after 230 s (not depicted).

current. The currently used (high) H^+ affinity is constrained by the experiments described in Hasenhuetl et al. (2016). However, we note that this is very likely an overestimation because, for the sake of simplicity, sequential H^+ binding was used.

Cl^- binding

Elevating internal Cl^- concentrations increased substrate-induced inward currents in cut-open *Xenopus laevis* oocyte preparations (Adams and DeFelice, 2003). Moreover, turnover rates were indistinguishable when Cl^- was increased from 0.5 to 143.5 mM in HEK293 cells using high internal K^+/H^+ concentrations (see Figs. 6–8 in Hasenhuetl et al., 2016). Erreger et al. (2008) introduced a parsimonious explanation for a similar phenomenon in DAT and suggested that Cl^- stays bound to the transporter during the entire catalytic cycle. Accordingly, we introduced this principle in a previous model (Hasenhuetl et al., 2016) and kept it for the present model. The rates of Cl^- binding were chosen such that the experimental data could be reproduced; there was no direct measurement of Cl^- affinity. It is reasonable to assume a cooperative binding scheme like that of Na^+ for Cl^- (Humphreys

Cooperative binding of Na^+ and substrate to SERT | Hasenhuetl et al.

Figure A4. **Turnover rates are independent of internal Cl⁻ concentration. (A)** Simulated peak current recovery experiment using 140 mM internal K^+ and 0.5 mM internal Cl^-. **(B)** Same protocol as in A, but using 152 mM internal Cl^-. The simulations reproduce data described in Hasenhuetl et al. (2016).
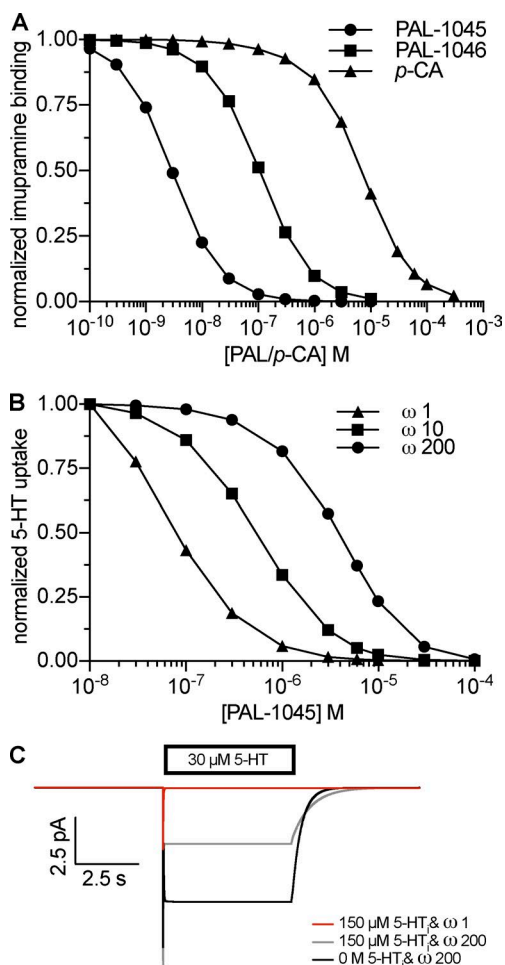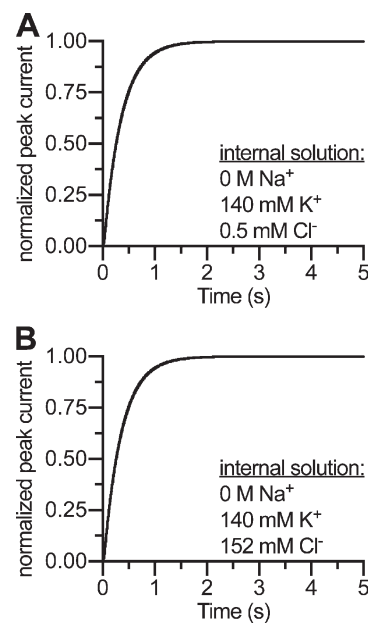
Figure A3. **Negative cooperativity between substrate and K^+. (A)** Simulation of radioligand binding at steady state. The simulations reproduce experimental data described in Bhat et al. (2017). The rates of imipramine binding were k_{on}, 5×10^6 M^{-1} s^{-1}; k_{off}, 0.015 s^{-1}. **(B)** Simulation of uptake inhibition using different negative cooperativity factors (ω values). The simulation using an ω value of 200 reproduces experimental data described in Bhat et al. (2017). **(C)** Simulated 5-HT–induced currents.

et al., 1994), but this was not a subject of this study. The simulated turnover rate was independent of internal Cl⁻ concentrations (Fig. A4) and is thus consistent with electrophysiological results (see Figs. 6–8 in Hasenhuetl et al., 2016).

ACKNOWLEDGMENTS

REFERENCES

Adams, S.V., and L.J. DeFelice. 2003. Ionic currents in the human serotonin transporter reveal inconsistencies in the alternating access hypothesis. *Biophys. J.* 85:1548–1559. https://doi.org/10.1016/S0006-3495(03)74587-1

Bhat, S., P.S. Hasenhuetl, A. Kasture, A. El-Kasaby, M.H. Baumann, B.E. Blough, S. Sucic, W. Sandtner, and M. Freissmuth. 2017. Conformational state interactions provide clues to the pharmacochaperone potential of serotonin transporter partial substrates. *J. Biol. Chem.* 292:16773–16786. https://doi.org/10.1074/jbc.M117.794081

Billesbølle, C.B., J.S. Mortensen, A. Sohail, S.G. Schmidt, L. Shi, H.H. Sitte, U. Gether, and C.J. Loland. 2016. Transition metal ion FRET uncovers K+ regulation of a neurotransmitter/sodium symporter. *Nat. Commun.* 7:12755. https://doi.org/10.1038/ncomms12755

Bönisch, H. 1986. The role of co-transported sodium in the effect of indirectly acting sympathomimetic amines. *Naunyn Schmiedebergs Arch. Pharmacol.* 332:135–141. https://doi.org/10.1007/BF00511403

Buchmayer, F., K. Schicker, T. Steinkellner, P. Geier, G. Stübiger, P.J. Hamilton, A. Jurik, T. Stockner, J.W. Yang, T. Montgomery, et al. 2013. Amphetamine actions at the serotonin transporter rely on the availability of phosphatidylinositol-4,5-bisphosphate. *Proc. Natl. Acad. Sci. USA.* 110:11642–11647. https://doi.org/10.1073/pnas.1220552110

Bulling, S., K. Schicker, Y.W. Zhang, T. Steinkellner, T. Stockner, C.W. Gruber, S. Boehm, M. Freissmuth, G. Rudnick, H.H. Sitte, and W. Sandtner. 2012. The mechanistic basis for noncompetitive ibogaine inhibition of serotonin and dopamine transporters. *J. Biol. Chem.* 287:18524–18534. https://doi.org/10.1074/jbc.M112.343681

Cheng, M.H., and I. Bahar. 2015. Molecular Mechanism of Dopamine Transport by Human Dopamine Transporter. *Structure.* 23:2171–2181. https://doi.org/10.1016/j.str.2015.09.001

Cremona, M.L., H.J. Matthies, K. Pau, E. Bowton, N. Speed, B.J. Lute, M. Anderson, N. Sen, S.D. Robertson, R.A. Vaughan, et al. 2011. Flotillin-1 is essential for PKC-triggered endocytosis and membrane microdomain localization of DAT. *Nat. Neurosci.* 14:469–477. https://doi.org/10.1038/nn.2781

Erreger, K., C. Grewer, J.A. Javitch, and A. Galli. 2008. Currents in response to rapid concentration jumps of amphetamine uncover novel aspects of human dopamine transporter function. *J. Neurosci.* 28:976–989. https://doi.org/10.1523/JNEUROSCI.2796-07.2008

Fog, J.U., H. Khoshbouei, M. Holy, W.A. Owens, C.B. Vaegter, N. Sen, Y. Nikandrova, E. Bowton, D.G. McMahon, R.J. Colbran, et al. 2006. Calmodulin kinase II interacts with the dopamine transporter C terminus to regulate amphetamine-induced reverse transport. *Neuron.* 51:417–429. https://doi.org/10.1016/j.neuron.2006.06.028

Gildea, J.J., P. Xu, J.M. Carlson, R.T. Gaglione, D. Bigler Wang, B.A. Kemp, C.M. Reyes, H.E. McGrath, R.M. Carey, P.A. Jose, and R.A. Felder. 2015. The sodium-bicarbonate cotransporter NBCe2 (slc4a5) expressed in human renal proximal tubules shows increased apical expression under high-salt conditions. *Am. J. Physiol. Regul. Integr. Comp. Physiol.* 309:R1447–R1459. https://doi.org/10.1152/ajpregu.00150.2015

Hamilton, P.J., A.N. Belovich, G. Khelashvili, C. Saunders, K. Erreger, J.A. Javitch, H.H. Sitte, H. Weinstein, H.J.G. Matthies, and A. Galli. 2014. PIP2 regulates psychostimulant behaviors through its interaction with a membrane protein. *Nat. Chem. Biol.* 10:582–589. https://doi.org/10.1038/nchembio.1545

Harootunian, A.T., J.P. Kao, B.K. Eckert, and R.Y. Tsien. 1989. Fluorescence ratio imaging of cytosolic free Na+ in individual fibroblasts and lymphocytes. *J. Biol. Chem.* 264:19458–19467.

Hasenhuetl, P.S., M. Freissmuth, and W. Sandtner. 2016. Electrogenic binding of intracellular cations defines a kinetic decision point in the transport cycle of the human serotonin transporter. *J. Biol. Chem.* 291:25864–25876. https://doi.org/10.1074/jbc.M116.753319

Hilber, B., P. Scholze, M.M. Dorostkar, W. Sandtner, M. Holy, S. Boehm, E.A. Singer, and H.H. Sitte. 2005. Serotonin-transporter mediated efflux: a pharmacological analysis of amphetamines and non-amphetamines. *Neuropharmacology.* 49:811–819. https://doi.org/10.1016/j.neuropharm.2005.08.008

Humphreys, C.J., S.C. Wall, and G. Rudnick. 1994. Ligand binding to the serotonin transporter: equilibria, kinetics, and ion dependence. *Biochemistry.* 33:9118–9125. https://doi.org/10.1021/bi00197a014

Kahlig, K.M., F. Binda, H. Khoshbouei, R.D. Blakely, D.G. McMahon, J.A. Javitch, and A. Galli. 2005. Amphetamine induces dopamine efflux through a dopamine transporter channel. *Proc. Natl. Acad. Sci. USA.* 102:3495–3500. https://doi.org/10.1073/pnas.0407737102

Kern, C., F.A. Erdem, A. El-Kasaby, W. Sandtner, M. Freissmuth, and S. Sucic. 2017. The N terminus specifies the switch between transport modes of the human serotonin transporter. *J. Biol. Chem.* 292:3603–3613. https://doi.org/10.1074/jbc.M116.771360

Keyes, S.R., and G. Rudnick. 1982. Coupling of transmembrane proton gradients to platelet serotonin transport. *J. Biol. Chem.* 257:1172–1176.

Khelashvili, G., S.G. Schmidt, L. Shi, J.A. Javitch, U. Gether, C.J. Loland, and H. Weinstein. 2016. Conformational dynamics on the extracellular side of LeuT controlled by Na+ and K+ ions and the protonation state of Glu290. *J. Biol. Chem.* 291:19786–19799. https://doi.org/10.1074/jbc.M116.731455

Khoshbouei, H., H. Wang, J.D. Lechleiter, J.A. Javitch, and A. Galli. 2003. Amphetamine-induced dopamine efflux. A voltage-sensitive and intracellular Na+-dependent mechanism. *J. Biol. Chem.* 278:12070–12077. https://doi.org/10.1074/jbc.M212815200

Korkhov, V.M., M. Holy, M. Freissmuth, and H.H. Sitte. 2006. The conserved glutamate (Glu136) in transmembrane domain 2 of the serotonin transporter is required for the conformational switch in the transport cycle. *J. Biol. Chem.* 281:13439–13448. https://doi.org/10.1074/jbc.M511382200

Kristensen, A.S., J. Andersen, T.N. Jørgensen, L. Sørensen, J. Eriksen, C.J. Loland, K. Strømgaard, and U. Gether. 2011. SLC6 neurotransmitter transporters: structure, function, and regulation. *Pharmacol. Rev.* 63:585–640. https://doi.org/10.1124/pr.108.000869

Läuger, P. 1991. Electrogenic Ion Pumps. Sinauer Associates, Sunderland, MA. 313 pp.

Lin, F., H.A. Lester, and S. Mager. 1996. Single-channel currents produced by the serotonin transporter and analysis of a mutation affecting ion permeation. *Biophys. J.* 71:3126–3135. https://doi.org/10.1016/S0006-3495(96)79506-1

Mager, S., C. Min, D.J. Henry, C. Chavkin, B.J. Hoffman, N. Davidson, and H.A. Lester. 1994. Conducting states of a mammalian serotonin transporter. *Neuron.* 12:845–859. https://doi.org/10.1016/0896-6273(94)90337-9

Mayer, F.P., A. Luf, C. Nagy, M. Holy, R. Schmid, M. Freissmuth, and H.H. Sitte. 2017. Application of a combined approach to identify new psychoactive street drugs and decipher their mechanisms at monoamine transporters. *Curr. Top. Behav. Neurosci.* 32:333–350. https://doi.org/10.1007/7854_2016_63

Menaker, D., A. Bendahan, and B.I. Kanner. 2006. The substrate specificity of a neuronal glutamate transporter is determined by the nature of the coupling ion. *J. Neurochem.* 99:20–28. https://doi.org/10.1111/j.1471-4159.2006.04003.x

Moritz, A.E., D.E. Rastedt, D.J. Stanislowski, M. Shetty, M.A. Smith, R.A. Vaughan, and J.D. Foster. 2015. Reciprocal phosphorylation and palmitoylation control dopamine transporter kinetics. *J. Biol. Chem.* 290:29095–29105. https://doi.org/10.1074/jbc.M115.667055

Nelson, P.J., and G. Rudnick. 1979. Coupling between platelet 5-hydroxytryptamine and potassium transport. *J. Biol. Chem.* 254:10084–10089.

Noskov, S.Y., and B. Roux. 2008. Control of ion selectivity in LeuT: two Na+ binding sites with two different mechanisms. *J. Mol. Biol.* 377:804–818. https://doi.org/10.1016/j.jmb.2008.01.015

Pizzo, A.B., C.S. Karam, Y. Zhang, H. Yano, R.J. Freyberg, D.S. Karam, Z. Freyberg, A. Yamamoto, B.D. McCabe, and J.A. Javitch. 2013. The membrane raft protein Flotillin-1 is essential in dopamine

neurons for amphetamine-induced behavior in Drosophila. *Mol. Psychiatry.* 18:824–833. https://doi.org/10.1038/mp.2012.82

Razavi, A.M., G. Khelashvili, and H. Weinstein. 2017. A Markov State-based Quantitative Kinetic Model of Sodium Release from the Dopamine Transporter. *Sci. Rep.* 7:40076. https://doi.org/10.1038/srep40076

Rodriguez-Menchaca, A.A., E. Solis Jr., K. Cameron, and L.J. De Felice. 2012. S(+)amphetamine induces a persistent leak in the human dopamine transporter: molecular stent hypothesis. *Br. J. Pharmacol.* 165:2749–2757. https://doi.org/10.1111/j.1476-5381.2011.01728.x

Rothman, R.B., J.S. Partilla, M.H. Baumann, C. Lightfoot-Siordia, and B.E. Blough. 2012. Studies of the biogenic amine transporters. 14. Identification of low-efficacy "partial" substrates for the biogenic amine transporters. *J. Pharmacol. Exp. Ther.* 341:251–262. https://doi.org/10.1124/jpet.111.188946

Sandtner, W., D. Schmid, K. Schicker, K. Gerstbrein, X. Koenig, F.P. Mayer, S. Boehm, M. Freissmuth, and H.H. Sitte. 2014. A quantitative model of amphetamine action on the 5-HT transporter. *Br. J. Pharmacol.* 171:1007–1018. https://doi.org/10.1111/bph.12520

Sandtner, W., T. Stockner, P.S. Hasenhuetl, J.S. Partilla, A. Seddik, Y.W. Zhang, J. Cao, M. Holy, T. Steinkellner, G. Rudnick, et al. 2016. Binding Mode Selection Determines the Action of Ecstasy Homologs at Monoamine Transporters. *Mol. Pharmacol.* 89:165–175. https://doi.org/10.1124/mol.115.101394

Schicker, K., Z. Uzelac, J. Gesmonde, S. Bulling, T. Stockner, M. Freissmuth, S. Boehm, G. Rudnick, H.H. Sitte, and W. Sandtner. 2012. Unifying concept of serotonin transporter-associated currents. *J. Biol. Chem.* 287:438–445. https://doi.org/10.1074/jbc.M111.304261

Schmidt, H., and M. Jirstrand. 2006. Systems Biology Toolbox for MATLAB: a computational platform for research in systems biology. *Bioinformatics.* 22:514–515. https://doi.org/10.1093/bioinformatics/bti799

Scholze, P., J. Zwach, A. Kattinger, C. Pifl, E.A. Singer, and H.H. Sitte. 2000. Transporter-mediated release: a superfusion study on human embryonic kidney cells stably expressing the human serotonin transporter. *J. Pharmacol. Exp. Ther.* 293:870–878.

Seidel, S., E.A. Singer, H. Just, H. Farhan, P. Scholze, O. Kudlacek, M. Holy, K. Koppatz, P. Krivanek, M. Freissmuth, and H.H. Sitte. 2005. Amphetamines take two to tango: an oligomer-based count-er-transport model of neurotransmitter transport explores the amphetamine action. *Mol. Pharmacol.* 67:140–151.

Sitte, H.H., and M. Freissmuth. 2015. Amphetamines, new psychoactive drugs and the monoamine transporter cycle. *Trends Pharmacol. Sci.* 36:41–50. https://doi.org/10.1016/j.tips.2014.11.006

Sitte, H.H., P. Scholze, P. Schloss, C. Pifl, and E.A. Singer. 2000. Characterization of carrier-mediated efflux in human embryonic kidney 293 cells stably expressing the rat serotonin transporter: a superfusion study. *J. Neurochem.* 74:1317–1324. https://doi.org/10.1046/j.1471-4159.2000.741317.x

Steinkellner, T., J.W. Yang, T.R. Montgomery, W.Q. Chen, M.T. Winkler, S. Sucic, G. Lubec, M. Freissmuth, Y. Elgersma, H.H. Sitte, and O. Kudlacek. 2012. Ca(2+)/calmodulin-dependent protein kinase IIα (αCaMKII) controls the activity of the dopamine transporter: implications for Angelman syndrome. *J. Biol. Chem.* 287:29627–29635. https://doi.org/10.1074/jbc.M112.367219

Steinkellner, T., L. Mus, B. Eisenrauch, A. Constantinescu, D. Leo, L. Konrad, M. Rickhag, G. Sørensen, E.V. Efimova, E. Kong, et al. 2014. In vivo amphetamine action is contingent on αCaMKII. *Neuropsychopharmacology.* 39:2681–2693. https://doi.org/10.1038/npp.2014.124

Steinkellner, T., T.R. Montgomery, T. Hofmaier, O. Kudlacek, J.W. Yang, M. Rickhag, G. Jung, G. Lubec, U. Gether, M. Freissmuth, and H.H. Sitte. 2015. Amphetamine action at the cocaine- and antidepressant-sensitive serotonin transporter is modulated by αCaMKII. *J. Neurosci.* 35:8258–8271. https://doi.org/10.1523/JNEUROSCI.4034-14.2015

Sucic, S., S. Dallinger, B. Zdrazil, R. Weissensteiner, T.N. Jørgensen, M. Holy, O. Kudlacek, S. Seidel, J.H. Cha, U. Gether, et al. 2010. The N terminus of monoamine transporters is a lever required for the action of amphetamines. *J. Biol. Chem.* 285:10924–10938. https://doi.org/10.1074/jbc.M109.083154

Tao, Z., and C. Grewer. 2007. Cooperation of the conserved aspartate 439 and bound amino acid substrate is important for high-affinity Na$^+$ binding to the glutamate transporter EAAC1. *J. Gen. Physiol.* 129:331–344. https://doi.org/10.1085/jgp.200609678

Zhao, Y., D. Terry, L. Shi, H. Weinstein, S.C. Blanchard, and J.A. Javitch. 2010. Single-molecule dynamics of gating in a neurotransmitter transporter homologue. *Nature.* 465:188–193. https://doi.org/10.1038/nature09057